



# Acute Pannexin 1 Blockade Mitigates Early Synaptic Plasticity Defects in a Mouse Model of Alzheimer's Disease

Carolina Flores-Muñoz<sup>1,2,3</sup>, Bárbara Gómez<sup>1,4</sup>, Elena Mery<sup>1,4</sup>, Paula Mujica<sup>1,2,3</sup>, Ivana Gajardo<sup>1</sup>, Claudio Córdova<sup>5</sup>, Daniela Lopez-Espíndola<sup>3,6</sup>, Claudia Durán-Aniotz<sup>7,8,9</sup>, Claudio Hetz<sup>8,9,10</sup>, Pablo Muñoz<sup>1,6</sup>, Arlek M. Gonzalez-Jamett<sup>2\*</sup> and Álvaro O. Ardiles<sup>1,2,11\*</sup>

<sup>1</sup>Centro de Neurología Traslacional, Facultad de Medicina, Universidad de Valparaíso, Valparaíso, Chile, <sup>2</sup>Centro Interdisciplinario de Neurociencia de Valparaíso, Universidad de Valparaíso, Valparaíso, Chile, <sup>3</sup>Programa de Doctorado en Ciencias, Mención Neurociencia, Universidad de Valparaíso, Valparaíso, Chile, <sup>4</sup>Escuela de Tecnología Médica, Facultad de Medicina, Universidad de Valparaíso, Valparaíso, Chile, <sup>5</sup>Laboratorio de Estructura y Función Celular, Facultad de Medicina, Universidad de Valparaíso, Valparaíso, Chile, <sup>6</sup>Centro de Investigaciones Biomédicas, Escuela de Medicina, Universidad de Valparaíso, Valparaíso, Chile, <sup>7</sup>Center for Social and Cognitive Neuroscience (CSCN), School of Psychology, Universidad Adolfo Ibáñez, Santiago de Chile, Chile, <sup>8</sup>Biomedical Neuroscience Institute, Faculty of Medicine, University of Chile, Santiago, Chile, <sup>9</sup>Center for Geroscience, Brain Health and Metabolism, Santiago, Chile, <sup>10</sup>Program of Cellular and Molecular Biology, Institute of Biomedical Sciences, University of Chile, Santiago, Chile, <sup>11</sup>Centro Interdisciplinario de Estudios en Salud, Facultad de Medicina, Universidad de Valparaíso, Viña del Mar, Chile

## OPEN ACCESS

### Edited by:

Hansen Wang,  
University of Toronto, Canada

### Reviewed by:

Carla Cannizzaro,  
University of Palermo, Italy  
Alain Buisson,  
Université Grenoble Alpes, France  
Nicola Origlia,  
Italian National Research Council,  
Italy

### \*Correspondence:

Arlek M. Gonzalez-Jamett  
arlek.gonzalez@cinv.cl  
Álvaro O. Ardiles  
alvaro.ardiles@uv.cl

**Received:** 05 October 2019

**Accepted:** 18 February 2020

**Published:** 19 March 2020

### Citation:

Flores-Muñoz C, Gómez B, Mery E, Mujica P, Gajardo I, Córdova C, Lopez-Espíndola D, Durán-Aniotz C, Hetz C, Muñoz P, Gonzalez-Jamett AM and Ardiles AO (2020) Acute Pannexin 1 Blockade Mitigates Early Synaptic Plasticity Defects in a Mouse Model of Alzheimer's Disease. *Front. Cell. Neurosci.* 14:46. doi: 10.3389/fncel.2020.00046

Synaptic loss induced by soluble oligomeric forms of the amyloid  $\beta$  peptide (sA $\beta$ os) is one of the earliest events in Alzheimer's disease (AD) and is thought to be the major cause of the cognitive deficits. These abnormalities rely on defects in synaptic plasticity, a series of events manifested as activity-dependent modifications in synaptic structure and function. It has been reported that pannexin 1 (Panx1), a nonselective channel implicated in cell communication and intracellular signaling, modulates the induction of excitatory synaptic plasticity under physiological contexts and contributes to neuronal death under inflammatory conditions. Here, we decided to study the involvement of Panx1 in functional and structural defects observed in excitatory synapses of the amyloid precursor protein (APP)/presenilin 1 (PS1) transgenic (Tg) mice, an animal model of AD. We found an age-dependent increase in the Panx1 expression that correlates with increased A $\beta$  levels in hippocampal tissue from Tg mice. Congruently, we also observed an exacerbated Panx1 activity upon basal conditions and in response to glutamate receptor activation. The acute inhibition of Panx1 activity with the drug probenecid (PBN) did not change neurodegenerative parameters such as amyloid deposition or astrogliosis, but it significantly reduced excitatory synaptic defects in the AD model by normalizing long-term potentiation (LTP) and depression and improving dendritic arborization and spine density in hippocampal neurons of the Tg mice. These results suggest a major contribution of Panx1 in the early mechanisms leading to the synaptopathy in AD. Indeed, PBN induced a reduction in the activation of p38 mitogen-activated protein kinase (MAPK), a kinase widely implicated in the early neurotoxic signaling in AD. Our data strongly suggest that an enhanced expression and activation of Panx1 channels contribute to the A $\beta$ -induced cascades leading to synaptic dysfunction in AD.

**Keywords:** pannexin 1, Alzheimer's disease, amyloid- $\beta$  peptide, synaptic plasticity, p38 mitogen-activated protein kinase (MAPK)

## INTRODUCTION

Alzheimer's disease (AD) is an age-dependent neurodegenerative disorder characterized by severe deterioration of cognitive functions leading to dementia (Selkoe, 2001). Classical neuropathological hallmarks of AD, such as intraneuronal accumulation of hyperphosphorylated Tau protein in neurofibrillary tangles or extracellular deposition of amyloid- $\beta$  peptide (A $\beta$ ) in senile plaques, have been considered as the culprit of neuronal damage; however, they show a weak correlation with memory loss (Selkoe, 2001; Nelson et al., 2012). Evidence from human brain studies suggests that the best correlate with cognitive deficits are synaptic loss and hippocampal volume reduction (DeKosky and Scheff, 1990; Terry et al., 1991; Morra et al., 2009; Peng et al., 2015). Accordingly, synaptic dysfunction and memory impairments have been reported in several animal models of AD before the appearance of neuropathological changes (Duyckaerts et al., 2008; Götz and Ittner, 2008; Philipson et al., 2010). In this regard, a number of evidences suggest that soluble oligomeric forms of A $\beta$  (sA $\beta$ os), identified in AD patients (Gong et al., 2003; Fukumoto et al., 2010) and AD animal models (Mucke et al., 2000; Price et al., 2014), precede the fibrillar amyloid deposition and tau pathology and have been implicated in the synaptopathy observed before the neurodegeneration appearance (Selkoe, 2008; Sheng et al., 2012). Congruently, sA $\beta$ os from different sources (i.e., synthetic, cell line-derived, human and mouse brain-derived) induce detrimental effects on memory (Cleary et al., 2005; Reed et al., 2011), synaptic morphology (Hsieh et al., 2006; Lacor et al., 2007; Shankar, 2007; Price et al., 2014) and glutamate receptor trafficking, expression and function (Snyder et al., 2005; Hsieh et al., 2006; Shankar, 2007; Miñano-Molina et al., 2011; Ardiles et al., 2012), and consequently, impair excitatory synaptic plasticity (Kim et al., 2001; Townsend et al., 2006; Klyubin et al., 2008; Shankar et al., 2008; Li et al., 2009).

Mechanisms underlying synaptic plasticity manifest as activity-induced long-lasting changes in the synaptic efficacy, which have been better characterized in the CA1 region of the hippocampus (Malenka and Bear, 2004). There, the most prominent forms of excitatory synaptic plasticity are long-term potentiation (LTP) and long-term depression (LTD) of the synaptic strength, which require the activation of N-methyl-D-aspartate receptors (NMDARs) and metabotropic glutamate receptors (mGluRs) for its induction (Malenka and Bear, 2004). Both LTP and LTD are expressed by changes in the trafficking, surface expression, and functionality of glutamate  $\alpha$ -amino-3-hydroxy-5-methyl-4-isoxazole propionic acid receptors (AMPA; Malenka and Bear, 2004) and have been proposed to be the molecular basis of learning and memory (Lynch, 2004; Collingridge et al., 2010; Takeuchi et al., 2014). These modifications in synaptic functionality are accompanied by structural rearrangements in the synaptic connections (Harris et al., 2003; Gogolla et al., 2007; Cingolani and Goda, 2008) manifested as changes in size, shape, and number of dendritic spines (Segal, 2005), which are critically dependent on the remodeling of the actin-cytoskeleton (Matus, 2000; Gordon-Weeks and Fournier, 2014). sA $\beta$ os have been

shown to affect both structural (Hsieh et al., 2006; Lacor et al., 2007; Shankar et al., 2008; Price et al., 2014) and functional synaptic plasticity (Kim et al., 2001; Townsend et al., 2006; Klyubin et al., 2008; Shankar et al., 2008; Li et al., 2009) by inhibiting LTP (Walsh et al., 2002; Wang et al., 2002) and enhancing NMDAR- (Kim et al., 2001; Hsieh et al., 2006; Li et al., 2009) and mGluR5-dependent LTD (Chen et al., 2013; Hu et al., 2014). sA $\beta$ os-induced LTP inhibition seems to involve excessive activation of extrasynaptic GluN2B-containing NMDARs (Li et al., 2011) and mGluR5s (Li et al., 2009) in a way dependent on the activation of Jun-N terminal kinase (JNK), Cdk5, and p38 mitogen-activated protein kinases (MAPKs; Wang et al., 2004; Li et al., 2011; Rammes et al., 2011) while sA $\beta$ os-induced LTD requires a metabotropic (non-ionotropic) function of GluN2B-containing NMDAR (Kessels et al., 2013; Tamburri et al., 2013) as well as activation of mGluR5 and their downstream signaling cascades including p38MAPK (Wang et al., 2004; Chen et al., 2013). Although sA $\beta$ os-induced signaling cascades are relatively well studied, the molecular mechanisms modulating these processes are still poorly understood. Recently, we reported that Panx1, a protein that forms functional nonselective channels in the plasma membrane and that is implicated in cell communication (MacVicar and Thompson, 2010), plays a critical role in modulating the neuronal activity in hippocampal synapses and in controlling the sliding threshold for excitatory synaptic plasticity (Ardiles et al., 2014). This Panx1 function appears to be induced by NMDAR and mGluR5, as glutamate receptors overactivation stimulates ATP release and promote hippocampal hyperactivity, which can be prevented by Panx1 blockers (Thompson et al., 2008; Lopatár et al., 2015). Remarkably, the application of exogenous A $\beta$  in acute hippocampal slices has been shown to induce neuronal death *via* increasing surface membrane expression and activity of Panx1 channels (Orellana et al., 2011b), strongly suggesting the involvement of Panx1 in the A $\beta$ -mediated neurotoxicity. With this in mind, we investigated the participation of Panx1 channels in the synaptic impairments observed in hippocampal tissue of amyloid precursor protein (APP)/presenilin 1 (PS1) transgenic (Tg) mice, a transgenic animal model of AD (Jankowsky et al., 2004). Specifically, we evaluated Panx1 expression and activity in hippocampal tissue of Tg mice and the impact of inhibiting its activity on neurodegeneration parameters, such as A $\beta$  deposition and astrogliosis, and on synaptic plasticity and neuronal structure. Our data show that Panx1 is overexpressed and overactive in Tg hippocampal tissue and that its expression correlates well with enhanced levels of the A $\beta$  peptide. The acute inhibition of Panx1 with probenecid (PBN) reverts the defects in synaptic plasticity and structure observed in hippocampal tissue of Tg mice but has no significant effects on neurodegeneration, suggesting that Panx1 activation plays a major role in the initial steps of the synaptopathy in AD. In fact, PBN significantly reduces the activation of p38MAPK, a kinase that reportedly enhances its expression and activity at early stages of AD (Sun et al., 2003), further supporting a role of Panx1 in the A $\beta$ -induced signaling that leads to the early synaptic dysfunction in AD.

## MATERIALS AND METHODS

### Animals

Unless otherwise noted, all experiments were carried out in 6-month-old (m.o.) C57BL/6 wild-type (Wt) or APP<sup>sw</sup>/PSEN1 $\Delta$ E9 mice (Tg mice). Tg mice, which express the mutant APP<sup>sw</sup> (K595N/M596L) and PSEN1 $\Delta$ E9, deletion of the exon 9 (APP/PS1 mice stock 004462), were obtained from Jackson Laboratory (Bar Harbor, ME, USA). Mice were housed at 22°C at constant humidity (55%), 12/12-h dark-light cycle, with a light phase from 8:00 AM to 8:00 PM. Food and water were provided *ad libitum*. The use and care of the animals were approved by the Ethics and Animal Care Committee of Universidad de Valparaíso (BEA064-2015).

### Drugs and Treatments

PBN and N-[N-(3,5-difluorophenacetyl-L-alanyl)]-S-phenylglycine t-butyl ester (DAPT) were obtained from Sigma Aldrich. SB203580 (SB) was kindly provided by Dr. Andrew Quest (Universidad de Chile). All other chemicals were purchased from Merck or Sigma. Drugs were applied in artificial cerebrospinal fluid (ACSF) as follows: After brain dissection, hemispheres (histology) or slices (electrophysiology and biochemistry) were maintained in ACSF bubbled with a mixture of 5% CO<sub>2</sub> and 95% O<sub>2</sub> plus vehicle [sodium hydroxide (NaOH), ethanol, and dimethyl sulfoxide (DMSO)] or drug (100  $\mu$ M PBN, 1  $\mu$ M SB, and 0.5  $\mu$ M DAPT) for 2 h.

### Excitatory Postsynaptic Field Recordings

Hippocampal slices were prepared as we previously reported (Ardiles et al., 2012; Gajardo et al., 2018). Briefly, mice were deeply anesthetized with isoflurane, brains quickly removed and hippocampus sectioned in slices of 350  $\mu$ m in ice-cold dissection buffer using a vibroslicer (Leica VT1200S, Leica Microsystems, Nussloch, Germany). After 1 h stabilization in ACSF (in mM: 119 NaCl, 26 NaHCO<sub>3</sub>, 1 NaH<sub>2</sub>PO<sub>4</sub>, 11 glucose, 2.5 KCl, 4 CaCl<sub>2</sub>, 4 MgCl<sub>2</sub>, 1.25 NaHPO<sub>4</sub>), slices were treated with 100  $\mu$ M PBN in ACSF for 2 h and then subjected to stimulation of the Schaffer collaterals using 0.2-ms pulses delivered through concentric bipolar stimulating electrodes and recorded extracellularly in the stratum radiatum of CA1. LTP was induced using four theta burst stimulations (TBSs; 10 trains of four pulses at 100 Hz; 5 Hz inter-burst interval) delivered at 0.1 Hz. LTD was induced using paired-pulse (50-ms interval) low-frequency stimulation (ppLFS; 900 pulses delivered at 1 Hz) in the presence or absence of PBN. LTP and LTD magnitudes were calculated as the average (normalized to baseline) of the responses recorded 50–60 min after conditioning stimulation.

### Synaptosomal Fractionation

Synaptosomes were extracted from hippocampus of 6 m.o. male mice as we previously described (Gajardo et al., 2018). Hippocampi were homogenized in ice-cold homogenization buffer [320 mM sucrose, 4 mM 4-(2-hydroxyethyl)-1-piperazineethanesulfonic acid (HEPES), and 1 mM ethylene glycol-bis( $\beta$ -aminoethyl ether)-N,N,N',N'-tetraacetic acid; EGTA], pH 7.4; protease and phosphatase inhibitor cocktails

using a Dounce tissue grinder. The homogenate was centrifuged at 1,000 $\times$  g for 10 min at 4°C (Beckman F0630 rotor) obtaining a supernatant (S1), which was collected, whereas the pellet (P1) was discarded. Then, S1 was centrifuged at 12,000 $\times$  g for 20 min at 4°C. The obtained pellet (P2) containing the membrane proteins was resuspended in homogenization buffer, layered on the top of a discontinuous sucrose density gradient (0.32/1.0/1.2 M) and subjected to ultracentrifugation at 165,000 $\times$  g (Beckman SW-60ti rotor) for 65 min at 4°C. Then, both the sediment and sucrose 0.32/1 M interface were discarded, whereas material accumulated at the interface of 1.0 M and 1.2 M sucrose-containing synaptosome (SP1) fraction was collected. SP1 was diluted with lysis buffer to restore the sucrose concentration to 320 mM and remained on ice with gentle agitation for 30 min. Then, SP1 was centrifuged at 33,000 $\times$  g (Beckman F0630 rotor) for 30 min. The pellet obtained (PS1) was resuspended in a gradient load buffer, loaded on 0.32/1.0/1.2 M discontinuous gradient, and centrifuged at 165,000 $\times$  g (Beckman SW-60ti rotor) for 65 min. The sucrose 1/1.2 M interphase, synaptosome fraction 2 (SP2), was recovered and delipidated in a delipidating buffer. Next, SP2 was diluted with a filling buffer to restore the sucrose concentration and then centrifuged at 33,000 $\times$  g (Beckman F0630 rotor) for 1 h. The sediment obtained (PS2) was washed with 50 mM HEPES-Na and centrifuged at 165,000 $\times$  g (Beckman SW-60ti rotor) for 10 min. The final sediment obtained (PS3), containing postsynaptic densities (PSDs), was resuspended in 50 mM HEPES-Na and homogenized. PS2 or PSD fractions were quantified for protein concentration and submitted to Western blot.

### Western Blot

Hippocampal slices (5–6 slices per animal; seven animals per group) from 3- to 12-months mice were frozen with dry ice and homogenized in lysis buffer [150 mM NaCl, 10 mM Tris-HCl, pH 7.4, ethylenediaminetetraacetic acid (EDTA) 2 mM, 1% Triton X-100, and 0.1% sodium dodecyl sulfate (SDS)], supplemented with a protease and phosphatase inhibitor cocktail (Thermo Fisher Scientific, Rockford, IL, USA) by using a glass-Potter homogenizer. Protein samples from whole homogenates or synaptosomal fractions were centrifuged twice for 10 min at 12,000 rpm at 4°C. Protein concentration was determined with the Qubit<sup>®</sup> Protein Assay Kit (Thermo Fisher Scientific, Rockford, IL, USA). For both cases, 40  $\mu$ g of protein per lane were resolved by 10% SDS-polyacrylamide gel electrophoresis (PAGE), followed by immunoblotting on polyvinylidene fluoride (PVDF) membranes (BioRad, Berkeley, CA, USA) and probed with specific antibodies against Panx1 (rabbit anti-Panx1, ABN242 Merck; 1:1,000), PSD-95 (mouse anti-PSD-95, MAB1596 Merck; 1:1,000), synaptophysin (goat anti-SYP, sc-9116, Santa Cruz Biotechnology, Santa Cruz, CA, USA; 1:2,000), p38 MAPK (rabbit anti-p38MAPK, #9212, Cell Signaling Technology, Danvers, MA, USA; 1:1,000), phospho-p38 MAPK (rabbit anti-Thr180/Tyr182, #9211, Cell Signaling Technology, Danvers, MA, USA; 1:1,000), and glyceraldehyde 3-phosphate dehydrogenase (GAPDH; mouse anti-GAPDH, sc-47724, Santa Cruz Biotechnology, Santa Cruz, CA, USA; 1:1,000). Band intensities were visualized by enhanced



chemiluminescence kit (ECL, BioRad, Berkeley, CA, USA), and the intensity of each band was scanned and densitometrically quantified using the ImageJ software (version 1.49v; National Institutes of Health, Bethesda, MD, USA).

sAβos were measured by a slot blot assays as previously described (Ardiles et al., 2012). Briefly, the total protein extract was centrifuged at 20,000 *g* for 1 h to eliminate fibrillar aggregates. The protein concentration of the soluble fraction was determined, and 6 mg of protein was spotted in 0.45-mm<sup>2</sup> nitrocellulose (Millipore, Kankakee, IL, USA), blocked with phosphate-buffered saline with Tween 20 (PBS-T) gelatin 0.4% and incubated using antibodies against total Aβ (6E10, BioLegend; 1:1,000) against oligomeric forms of Aβ (A11; rabbit anti-oligomer, AHB0052, Sigma, 1:5,000) and against Panx1 (rabbit anti-Panx1, ABN242, Merck; 1:1,000). Slot blots were then processed as mentioned above.

## Histology

For histological studies, mice were transcardially perfused with 0.9% NaCl and 4% paraformaldehyde (PFA) in phosphate buffer pH 7.4. For immunohistochemistry, paraffin-embedded brain tissue was cut into 7-μm sections using a cryostat (Leica CM1900) and treated for endogenous peroxidase blockade (3% hydrogen peroxide) followed by CAS-Block (Invitrogen, 008120) and blocking solution (5% goat serum, 0.3% Tween 20 in PBS). Tissues were incubated with primary rabbit anti-Panx1 antibody (ABN242, Merck; 1:200), mouse anti-glial fibrillary acidic protein (GFAP; clone 2E1, Santa Cruz Biotechnology, Santa Cruz, CA, USA; 1:500), and mouse anti-amyloid peptide antibody (clone 6E10, BioLegend; 1:1,000), followed by horseradish peroxidase (HRP)-linked secondary goat anti-mouse or anti-rabbit antibody (Thermo Fisher Scientific, Waltham, MA, USA; 1:250) and diaminobenzidine substrate (Sigma D5637) or p-nitroblue tetrazolium chloride (NBT)/5-bromo-4-chloro-3'-indolylphosphate p-toluidine (BCIP) (Thermo 34042) to visualization of peroxidase or alkaline phosphatase reactions, respectively. Additionally, brain sections were co-stained with Congo red (5%, Sigma) to mark amyloid material or counterstained with Nissl or Klüver–Barrera stains. Images were acquired in an upright microscope (Leica DM500) attached to a Leica ICC50W camera.

For immunofluorescence, 20-μm sections were stained with primary rabbit anti-Panx1 antibody (ABN242, Merck; 1:100), rabbit anti-GFAP (Z0334, DAKO; 1:500), rabbit anti-NeuN (AB177487, Abcam; 1:500), mouse anti-Panx1 antibody (MAB7097, R&D Systems; 1:200), mouse anti-GFAP (clone 2E1, Santa Cruz; 1:250), and mouse anti-amyloid peptide antibody (clone 6E10, BioLegend; 1:500), followed by cyanine-conjugated secondary goat anti-mouse or anti-rabbit antibodies (Jackson ImmunoResearch; 1:500). Additionally, brain sections were co-stained with 4',6-diamidino-2-phenylindole (DAPI, Sigma; 1:1,000) to label nuclei. Images were acquired in a confocal microscope (upright Eclipse Nikon 80i) using an immersion-oil Plan Fluor 100× magnification objective (NA 1.3) and identical exposure settings between compared samples. The astrocytic burden was measured by estimating the area of

GFAP immunostaining regarding the total area (*N* = 5–6 fields from three to four animals per group).

## Ethidium Bromide Uptake Assay

To test the activity of Panx1 channels under basal or glutamate receptor activation conditions, hippocampal slices were stabilized in a chamber with oxygenated ACSF (95% O<sub>2</sub> and 5% CO<sub>2</sub>) pH 7.4 for 1 h and then incubated with 20 μM of ethidium bromide (EtBr) for 5 min in ACSF only or in the presence of 50 μM of NMDA or 100 μM (S)-3,5-dihydroxyphenylglycine (DHPG). To test the activity of Panx1 and the effect of p38MAPK or γ-secretase inhibitors, hippocampal slices were stabilized for 2 h in the presence of PBN, the p38 MAPK inhibitor SB, or the γ-secretase inhibitor DAPT and their respective vehicles and then incubated with 20 μM of EtBr for 5 min in ACSF. After that, the slices were washed three times during 15 min with ACSF, fixed at room temperature with 4% PFA and 15% sucrose for 30 min, and maintained in PBS buffer. Then, slices were cut into 25-μm sections using a cryostat (Leica CM1900). The sections were stained with primary mouse anti βIII tubulin (clone 5G8, Promega; 1:1,000), rabbit anti-GFAP (Z0334, DAKO; 1:1,000), or mouse anti-NeuN (MAB377, Merck; 1:200), followed by cyanine-conjugated secondary goat anti-mouse or anti-rabbit antibodies (Jackson ImmunoResearch; 1:500). Mounted sections were examined in an Olympus IX81 Custom microscope coupled to an Olympus F-View Monochromatic CCD camera. Images were acquired with a 20× objective using Xcellence Pro software and processed with a custom-made algorithm based on Fiji (ImageJ software). Dye uptake ratio was calculated as the mean fluorescence intensity of the population of positive β-III tubulin or NeuN cells and normalized to the Wt group. At least three fields were selected in every slice.

## Golgi Staining to Dendritic Morphology Visualization

Dissected mouse brains were maintained for 2 h at room temperature in ACSF bubbled with a mixture of 5% CO<sub>2</sub> and 95% O<sub>2</sub> in the presence or the absence of 100 μM PBN and then processed for Golgi impregnation following manufacturer's instructions (FD NeuroTechnologies, Columbia, MD, USA). Coronal sections of 150-μm-thick brain slices were obtained using a semiautomatic cryostat microtome (Kedee KD-2950, Germany) at –20°C and mounted on gelatin-coated slides, developed with solutions of the same kit, dehydrated with a growing battery of alcohols (50–100%), and mounted using Entellan media (Millipore-Sigma, Germany). Images of pyramidal hippocampal neurons were acquired by a Leica Application Suite X (LASX, Leica Microsystems Inc., Buffalo Grove, IL, USA) under bright-field microscopy at 40× or 100× magnification using similar light conditions between experimental groups. Images were digitalized in 1,200 × 1,200 dpi resolution for morphometric analysis.

## Morphometric Analysis

Well-impregnated CA1 pyramidal neurons which had their branching isolated from surrounding neurons and their soma

located in the middle third of the tissue were used for analysis. Camera lucida drawings were performed using a 40× objective (Leica M80 attached to Leica DM500). Analysis of the camera lucida drawings were traced using the NeuronJ plugin and then quantified using Sholl analysis macro ImageJ (NIH, Bethesda, MD, USA). Dendritic branching was quantified as the number of intersections with concentric circles at increasing diameters (20- $\mu$ m steps) placed around the cell body. Dendritic length and spine number were analyzed at 20  $\mu$ m in Sholl analysis. All morphological analyses were performed blind to the experimental conditions.

### Statistical Analysis

Data are shown as mean  $\pm$  standard error of the mean (SEM). Statistical analysis was performed using GraphPad Prism (GraphPad Software Inc., San Diego, CA, USA). Normality distribution of raw data was probed by Shapiro–Wilk test. Unpaired, two-tailed Student's *T*-tests or Mann–Whitney rank test for two sample comparison, ANOVA followed by Tukey's or Bonferroni's *post hoc* test, or Kruskal–Wallis followed by a Dunn's correction for multiple comparisons were performed to determine significant differences.

## RESULTS

### Pannexin 1 Expression and Activity in Transgenic Mouse Hippocampal Tissue

Panx1 is expressed in several brain areas including neocortex, hippocampus, amygdala, substantia nigra, olfactory bulb, and cerebellum with an age-dependent pattern (Vogt et al., 2005; Ardiles et al., 2014), showing higher levels in embryonic and young tissue, but declining during adulthood (Vogt et al., 2005; Ardiles et al., 2014). To evaluate whether Panx1 expression and distribution were altered in Tg brains, we performed Western blots from whole hippocampal homogenates using tissue from 3- to 12-m.o. Wt and Tg mice (**Figure 1A**). First, we confirmed that Panx1 expression was reduced during aging in Wt animals. Similarly, Tg also showed an age-dependent reduction, but reaching a peak of expression at 6 m.o. and decreasing after that. However, the expression of Panx1 was greater in whole hippocampal lysates from Tg compared to Wt mice in all the age ranges (**Figure 1A**). Moreover, a tendency to greater levels of Panx1 was observed in hippocampal synaptosome-enriched fractions isolated from 6-m.o. Tg compared to the Wt brains (**Supplementary Figure S1A**). Interestingly, the increased Panx1 expression observed in Tg hippocampal tissue significantly correlated with the age-dependent rising levels of A $\beta$  in Tg samples estimated by slot blot experiments using the 6E10 antibody (**Figure 1B**). Instead, an inverse and nonsignificant correlation between Panx1/A $\beta$  expressions was found in Wt samples (**Figure 1B**). Similar results were obtained when the anti-oligomer A11 antibody was used to detect A $\beta$  (**Supplementary Figure S1B**). Since Panx1 has been shown to be expressed not only in pyramidal neurons but also in interneurons and astrocytes (Vogt et al., 2005; Huang et al., 2007), we evaluated whether this increased Panx1 expression was given in neuronal or glial cells. As shown in **Figure 1C**, Panx1 reactivity in

hippocampal slices was observed in both NeuN-positive neurons and GFAP-positive astrocytes (**Figure 1C**). In fact, Panx1-positive astrocytes were significantly more in Tg slices compared to Wt animals (**Supplementary Figure S1C**). Interestingly, Panx1 exhibited a punctate staining pattern around amyloid plaques, in the pyramidal cell layer, neuropil, and reactive astrocytes (**Supplementary Figure S1D**), in agreement with previous observations that Panx1 is expressed in reactive astrocytes that are in direct contact with amyloid plaques in this AD model (Yi et al., 2016). These data strongly suggest that Panx1 is overexpressed in the hippocampal tissue of the Tg mice. In order to evaluate whether this augmented Panx1 expression associated with an enhanced Panx1 activity, we performed dye uptake experiments in hippocampal slices from Wt and Tg mice using EtBr in the presence of La<sup>+3</sup> to block the uptake through connexin hemichannels (Orellana et al., 2011b). As shown in **Figure 1D**, we observed an increased EtBr fluorescence in hippocampal slices from Tg compared to Wt animals upon basal conditions, which was reduced in the presence of PBN, a Panx1 blocker (Silverman et al., 2008; **Figure 1D**). Similarly, when we stimulated hippocampal slices with NMDA and DHPG to induce NMDARs and mGluR5 overactivation, we observed a higher EtBr fluorescence in hippocampal slices from Tg compared to Wt tissue (**Figure 1E**). PBN significantly decreased EtBr fluorescence in both Wt and Tg slices, indicating that dye uptake was through Panx1 channels. Together, these data suggest that, in the AD context, NMDAR and mGluR5 activation induces an exacerbated Panx1 activity.

### Pannexin 1 Blockade With Probenecid Does Not Affect Neurodegeneration-Related Events in Transgenic Mice

Along with amyloid plaques and neurofibrillary tangles, abnormal inflammation including reactive gliosis is one of the neuropathological hallmarks of AD (Selkoe, 2001). In fact, activated astrocytes and microglia surrounding amyloid plaques have been shown in AD brains (McGeer and McGeer, 2003). Accordingly, an increased GFAP staining has been previously reported in this AD model at 6 m.o. (Gomez-Arboledas et al., 2018). Considering that Panx1 channels have been involved in inflammatory conditions (Zhou K. Q. et al., 2019), playing a role in the inflammasome activation in astrocytes and neurons (Silverman et al., 2009), and since PBN appears to exert an anti-inflammatory effect by inhibiting Panx1 activity (Wei et al., 2015; Hainz et al., 2017; Zhang et al., 2019), we evaluated the effect of PBN on sA $\beta$ os accumulation, amyloid plaques, and GFAP immunoreactivity in Wt and Tg brains (**Figure 2**). Hippocampal slices were treated during 2 h with 100  $\mu$ M of PBN and then processed for the evaluation of neurodegeneration parameters. As shown in **Figure 2A**, sA $\beta$ os levels, estimated by the A11 antibody, were elevated in whole hippocampal lysates from Tg compared to Wt mice (**Figure 2A**). Treatment with PBN did not have a significant effect on this A $\beta$  accumulation (**Figure 2A**). Congo red-positive amyloid plaques were present in the hippocampus and adjacent cortex of Tg

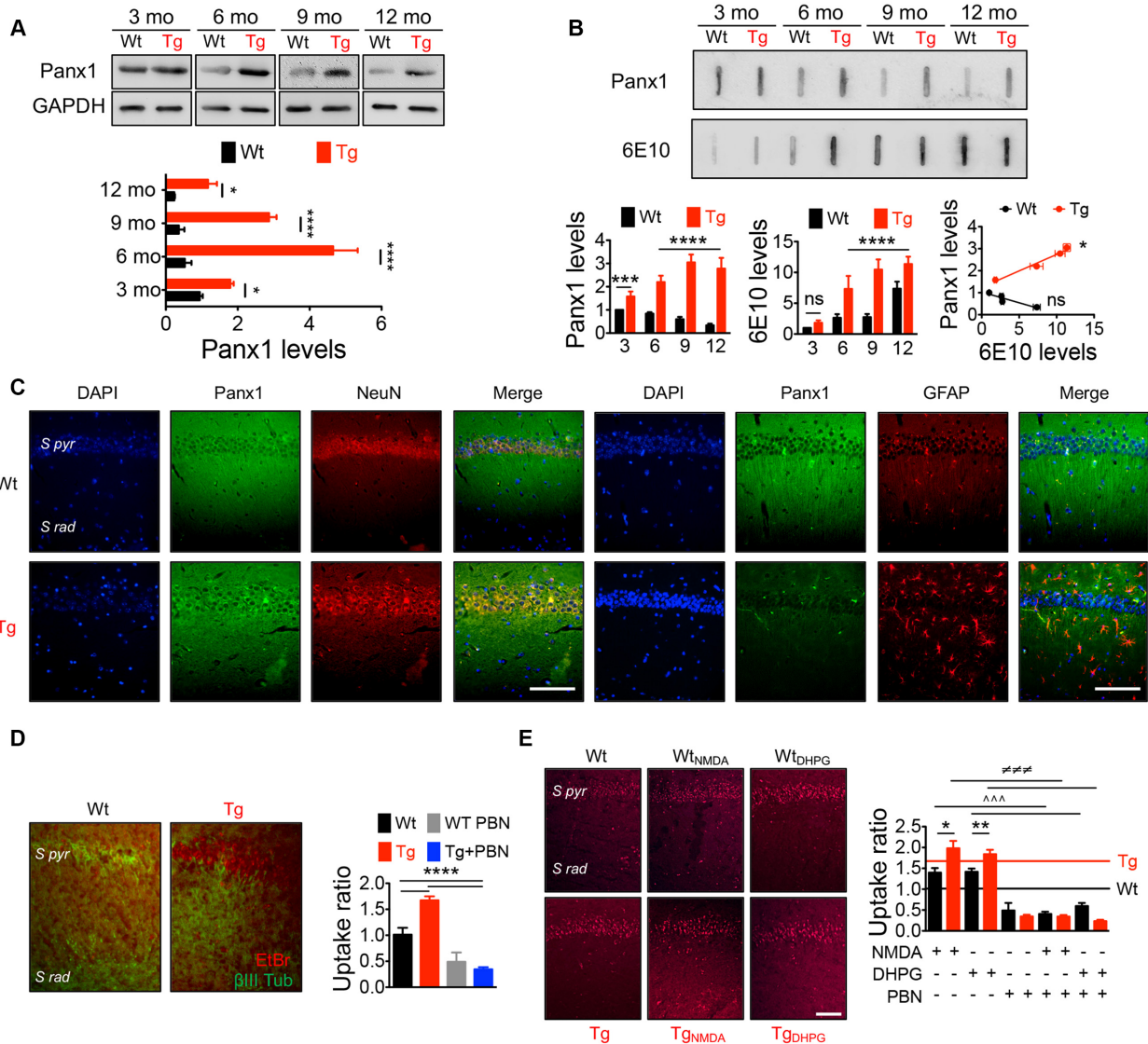
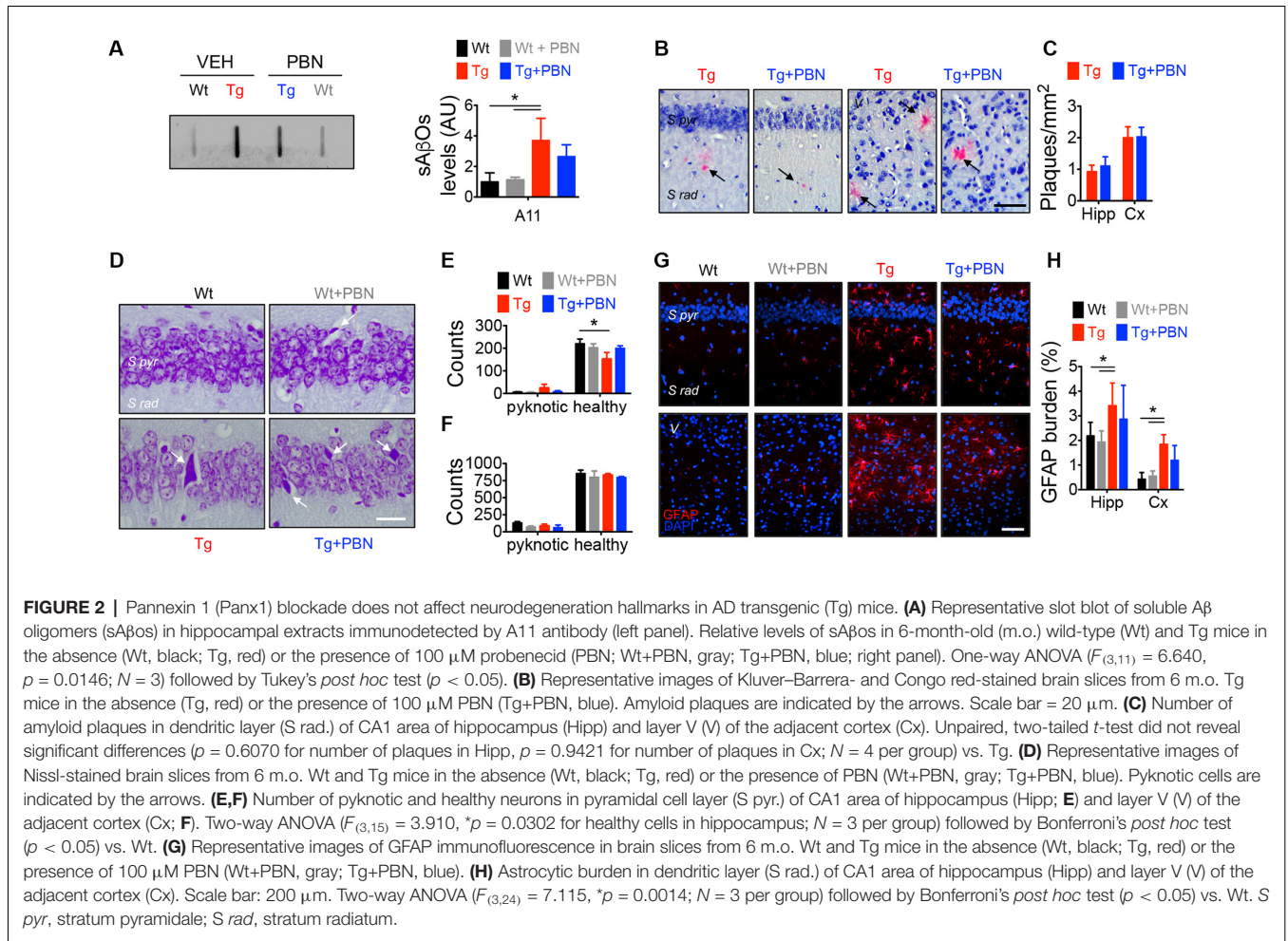


**FIGURE 1 |** Increased Pannexin 1 (Panx1) expression and activity in the hippocampus of Alzheimer's disease (AD) transgenic (Tg) mice. **(A)** Representative blots of Panx1 expression levels in whole hippocampal homogenates of wild-type (Wt, black) and Tg (red) mice at 3, 6, 9, and 12 months old (m.o.; Top panel). Western blot analysis of Panx1 levels normalized to glyceraldehyde 3-phosphate dehydrogenase (GAPDH) levels (bottom panel). Two-way ANOVA ( $F_{(3,48)} = 106.3$ ;  $p < 0.0001$ ) for age; ( $F_{(1,48)} = 771.4$ ;  $p < 0.0001$ ) for genotype.  $**p = 0.0053$  for 3 m.o.;  $****p < 0.0001$  for 6 m.o.;  $****p < 0.0001$  for 9 m.o.;  $**p = 0.0005$  for 12 m.o.; ( $N = 7$  animals per group) vs. Wt. **(B)** Representative slot blot of Panx1 and total amyloid- $\beta$  (A $\beta$ ) levels immunodetected by 6E10 antibody (6E10 levels) in hippocampal homogenates of Wt and Tg mice at 3, 6, 9, and 12 m.o. (Top panel). Slot blot analysis of Panx1 (left panel) and 6E10 (middle panel) levels and correlation between Panx1 and 6E10 levels at the different ages (right panel). Two-way ANOVA ( $F_{(3,48)} = 11.96$ ;  $p < 0.0001$ ) for age; ( $F_{(1,48)} = 652.4$ ;  $p < 0.0001$ ) for genotype.  $****p < 0.0001$ ;  $N = 7$  animals per group) for Panx1 levels, followed by Bonferroni's *post hoc* test ( $p < 0.005$ ). Two-way ANOVA [ $F_{(3,40)} = 99.60$ ;  $p < 0.0001$ ] for age; ( $F_{(1,40)} = 167.3$ ;  $p < 0.0001$ ) for genotype.  $**p = 0.0037$ ;  $***p = 0.0004$ ;  $****p < 0.0001$ ;  $N = 6$  animals per group) for levels 6E10, followed by Bonferroni's *post hoc* test ( $p < 0.005$ ). Two-way ANOVA ( $F_{(3,30)} = 23.43$ ;  $p < 0.0001$ ) for age; ( $F_{(1,10)} = 22.16$ ;  $p = 0.0008$ ).  $***p = 0.0004$ ;  $**p = 0.0013$ ;  $*p = 0.0260$ ;  $N = 6$  animals per group) for 6E10 levels, followed by Bonferroni's *post hoc* test ( $p < 0.005$ ). Correlation ( $r^2 = 0.9725$ ;  $*p = 0.0138$ ; for Tg;  $r^2 = 0.8560$ ;  $ns\rho = 0.0748$ ; for Wt); **(C)** Representative images showing the colocalization between Panx1 (green) and NeuN or glial fibrillary acidic protein (GFAP; red) immunoreactivity in the hippocampal CA1 area from 6 m.o. Wt and Tg mice. Scale bar = 50  $\mu$ m. **(D)** Representative images of ethidium bromide (EtBr) uptake by pyramidal neurons from hippocampal CA1 area treated with 200  $\mu$ M  $\text{La}^{3+}$  under resting conditions in the presence or absence of 100  $\mu$ M of probenecid (PBN; left panel). EtBr uptake ratio normalized to Wt group (right panel). One-way ANOVA ( $F_{(3,33)} = 47.29$ ;  $p < 0.0001$ ) for treatment;  $***p < 0.0001$  ( $N = 3$  animals per group) vs. Wt or Tg, followed by Bonferroni's *post hoc* test ( $p < 0.005$ ). S pyr, stratum pyramidale; S Rad, stratum radiatum. **(E)** Representative images of EtBr uptake by pyramidal neurons from hippocampal CA1 area treated with 200  $\mu$ M  $\text{La}^{3+}$  and stimulated with 50  $\mu$ M N-methyl-D-aspartate (NMDA) or 100  $\mu$ M (S)-3,5-dihydroxyphenylglycine (DHPG) in the presence or absence of 100  $\mu$ M of PBN (left panel). EtBr uptake ratio normalized to Wt group in resting conditions (**D**; right panel). Wt (black line) and Tg (red line) values obtained in resting conditions are indicated. One-way ANOVA ( $F_{(11,153)} = 68.82$ ;  $p < 0.0001$ )  $**p = 0.087$ ; ( $N = 3$  animals per group) vs. Wt<sub>NMDA</sub>;  $**p = 0.041$ , vs. Wt<sub>DHPG</sub>;  $^^^p < 0.0001$ , vs. Wt<sub>NMDA</sub> or Wt<sub>DHPG</sub>;  $^\#\#\#p < 0.0001$  ( $N = 3$  animals per group) vs. Tg<sub>NMDA</sub> or Tg<sub>DHPG</sub>, followed by Bonferroni's *post hoc* test ( $p < 0.005$ ). Scale bar = 50  $\mu$ m.





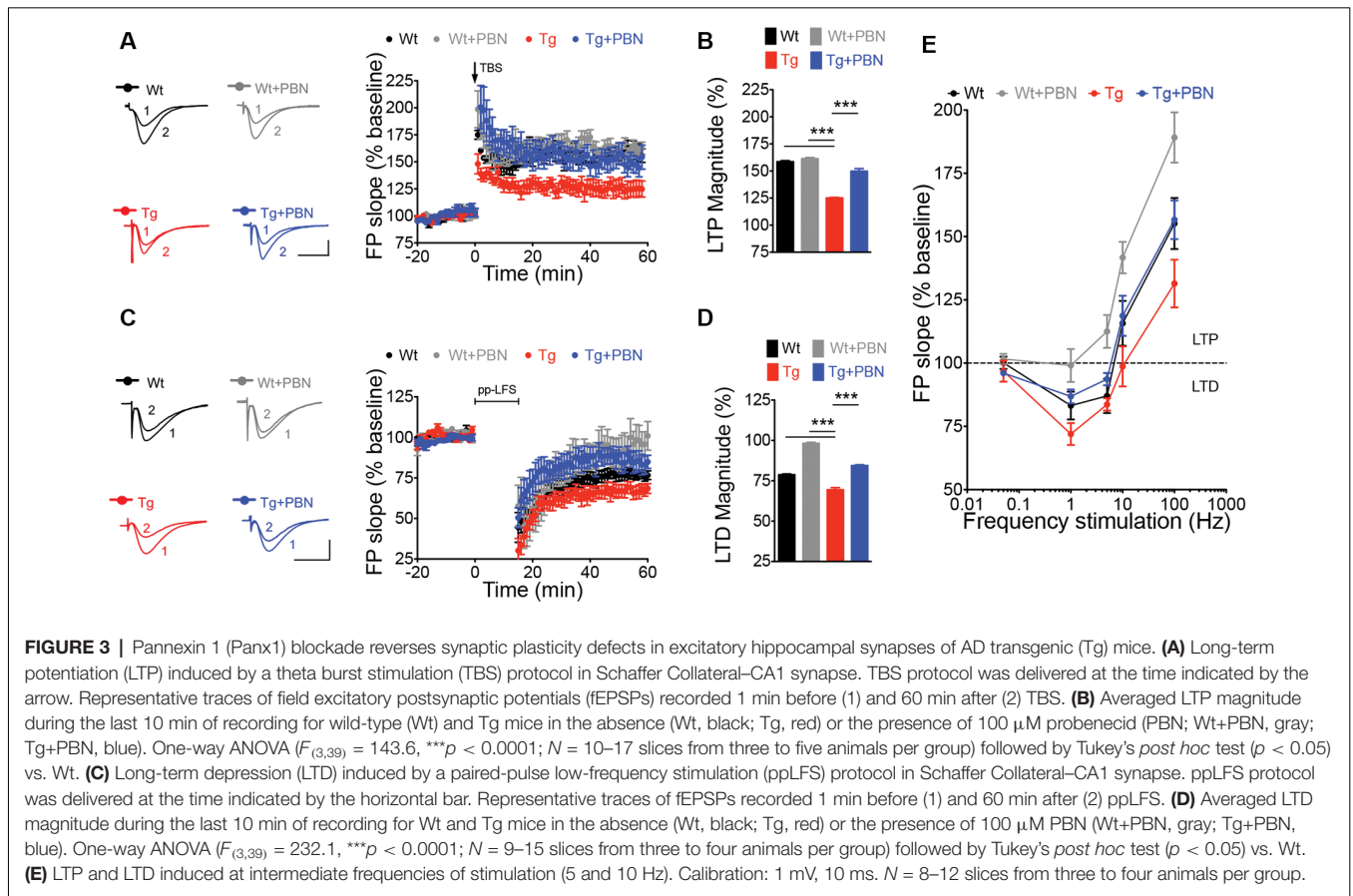
mice but were absent in Wt brains (**Figure 2B**). PBN treatment did not significantly affect the number of amyloid plaques (**Figures 2B,C**). As previously reported (Gomez-Arboledas et al., 2018), the GFAP-stained area was significantly increased in the hippocampus and adjacent cortex of Tg mice compared to Wt mice (**Figures 2G,H** and **Supplementary Figure S2A**), indicative of an augmented astrogliosis. However, treatment with PBN did not affect the percentage of reactive astrocytes (**Figure 2H**). Similarly, PBN had no effect on the reduced number of neurons in the CA1 pyramidal cell layer and adjacent cortex of Tg mice (**Figures 2D,E**), indicating that, at least during the 2 h of treatment, there was no impact on neuronal death.

Together, these data indicate that the acute blockade of Panx1 with PBN is not able to interfere with the toxic events associated with the neurodegenerative process in the AD context and suggest that Panx1 overactivation could have a more important role in earlier mechanisms.

### Pannexin 1 Blockade With Probenecid Normalizes Hippocampal Synaptic Plasticity in Transgenic Mice

LTP and LTD of the excitatory synaptic strength, the more prominent forms of synaptic plasticity, have been proposed to

be the molecular basis of learning and memory (Lynch, 2004; Collingridge et al., 2010; Takeuchi et al., 2014). One of the earliest processes induced by the A $\beta$  signaling in AD is an enhanced glutamate transmission (Palop et al., 2007; Busche et al., 2012) that produces an imbalance in the excitatory synaptic plasticity, impairing LTP, favoring LTD, and leading to synaptic dysfunction (Kim et al., 2001; Walsh et al., 2002; Wang et al., 2002; Hsieh et al., 2006; Li et al., 2009). This latter has been suggested as an initial stage of the disease that correlates well with the early cognitive decline in AD (Forner et al., 2017). Therefore, we analyzed the impact of interfering with Panx1 overactivity on LTP/LTD in acute hippocampal slices of the Tg mice. To do that, we induced synaptic plasticity in hippocampal slices from 6 m.o. mice applying standard theta burst (TBS) and ppLFS protocols to induce LTP and LTD, respectively (Ardiles et al., 2014). Slices were incubated in the presence or absence of 100  $\mu$ M PBN during 2 h before synaptic plasticity induction. As shown in **Figure 3**, Tg hippocampal slices exhibited impaired LTP and LTD as compared to Wt slices (**Figures 3A,C**). The treatment with PBN modified excitatory synaptic responses in Tg slices, reducing LTD and increasing LTP, reaching values comparable to those observed in Wt slices (**Figures 3B,D**). At intermediate frequencies of stimulation (5 and 10 Hz), PBN



produced similar effects, demonstrating that the Pannx1 blockade changes the threshold for synaptic modifications in the AD model (Figure 3E). These data support the hypothesis that Pannx1 overactivation is involved in the synaptic dysfunction early induced by sA $\beta$ os.

### Pannexin 1 Blockade With Probenecid Improves Dendritic Morphology and Spine Density in the Hippocampus of Transgenic Mice

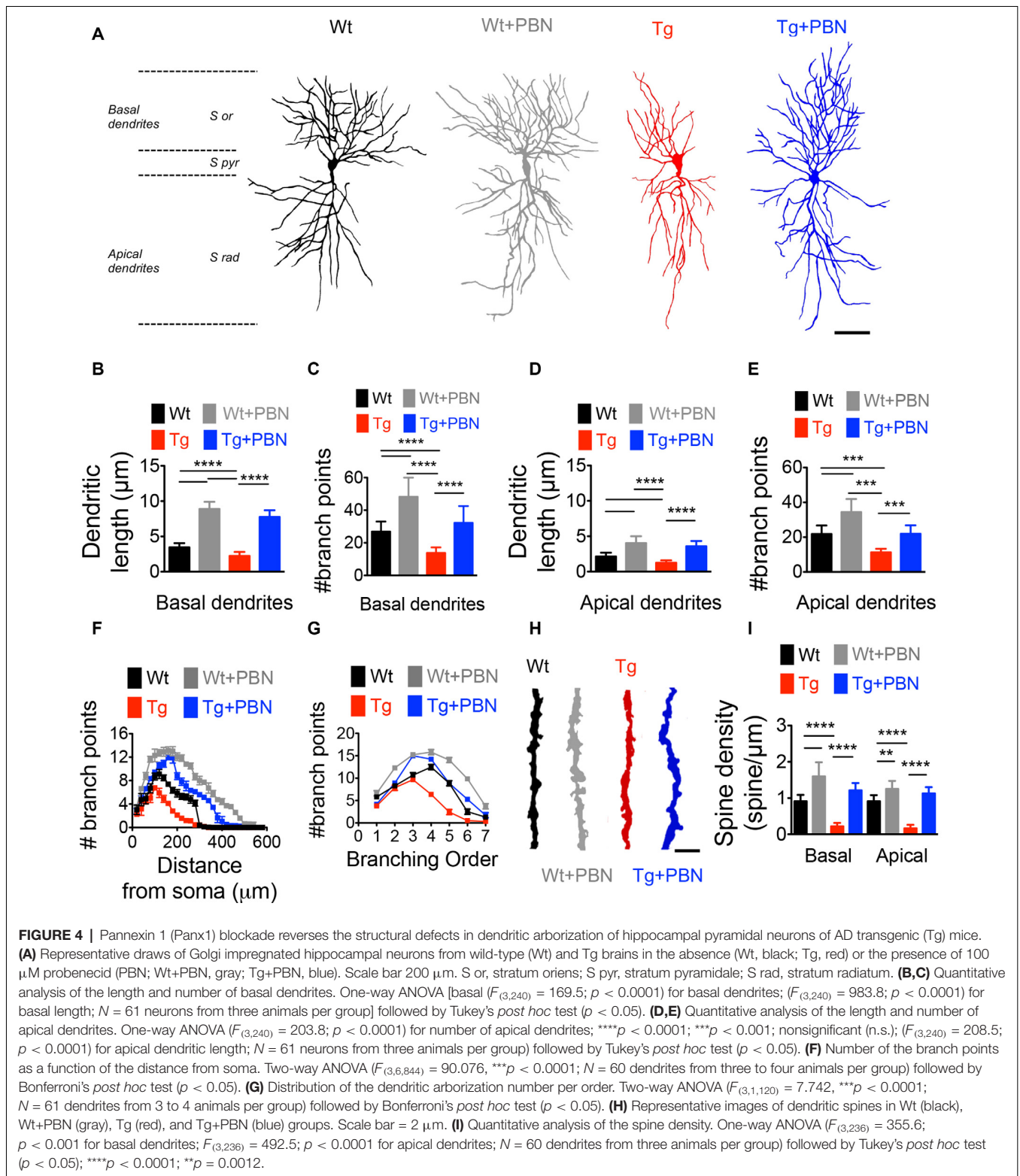
Activity-dependent modifications in the efficacy of the excitatory synaptic transmission require not only functional changes associated with the trafficking and activity of glutamate receptors but also structural remodeling of the dendritic morphology supporting rearrangements in the synaptic connections (Harris et al., 2003; Gogolla et al., 2007; Cingolani and Goda, 2008). To investigate whether the effect of PBN in the excitatory hippocampal synaptic plasticity in the AD model relies on structural synaptic modifications, we performed Golgi–Cox staining and obtained camera lucida drawings of hippocampal neurons from 6 m.o. of Wt and Tg mice and evaluated dendritic arborization as well as spine density. As shown in Figure 4, Tg pyramidal neurons exhibited a reduction in the dendritic complexity and spine density of CA1 neurons (Figure 4). The total length and the number of branch points of basal and apical

dendrites (Figures 4B–E), as well as the dendritic branching throughout the distance from soma (Figure 4F), the branch order (Figure 4G) and the spine density (Figures 4H,I) were significantly lower in Tg hippocampal neurons compared to Wt neurons. Remarkably, PBN antagonized all these effects, suggesting that Pannx1 plays a critical role in the early structural synaptic defects observed in the hippocampal tissue of Tg brains. It is noteworthy that PBN also increased dendritic arborization and spine density in hippocampal neurons from Wt animals, further indicating that Pannx1 blockade promotes structural changes in neuronal and synaptic morphology.

### The Blockade of Pannexin 1 With Probenecid Reduces p38 Mitogen-Activated Protein Kinase Overactivation in Transgenic Hippocampal Tissue

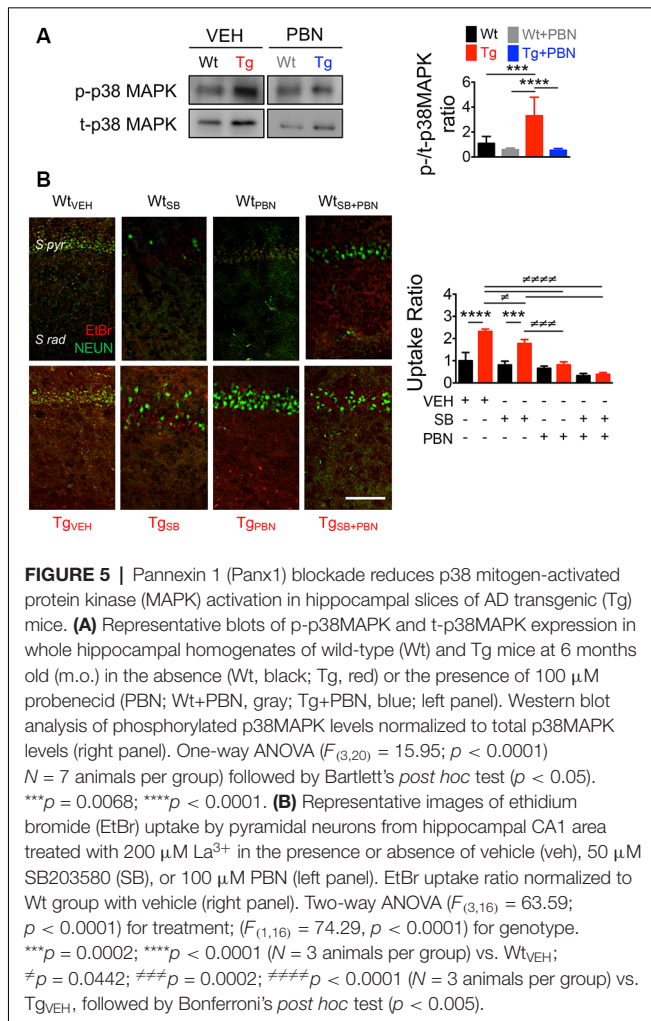
A number of evidences demonstrate that the tau-kinase p38MAPK becomes overactive during normal aging as well as in age-related neurodegenerative diseases such as AD (Hensley et al., 1999). Particularly, p38 $\alpha$ -MAPK appears to mediate early neuroinflammation, synaptic dysfunction, and spatial memory defects in AD models (Munoz et al., 2007). In fact, p38 $\alpha$ -MAPK inhibition reduces the microglial production of pro-inflammatory cytokines, improving synaptic and cognitive





functions in A $\beta$ -treated mice (Munoz et al., 2007) and genetic AD models (Roy et al., 2015). In order to analyze whether the role of Panx1 in the synaptic dysfunction in Tg hippocampal tissue relies on the overactivation of p38MAPK, we measured the

levels of p38MAPK phosphorylation (p-p38MAPK) in response to the PBN treatment. As shown in **Figure 5A**, p-p38MAPK was dramatically higher in Tg-total hippocampal lysates compared to the Wt condition. Treatment with PBN significantly reduced



p38MAPK phosphorylation, reaching values indistinguishable to those observed in the Wt tissue (**Figure 5A**). These data strongly suggest that Panx1 activity is an upstream regulator of the p38MAPK signaling in AD. To evaluate whether p38MAPK also influences Panx1 activation, we treated Wt and Tg hippocampal slices with the p38MAPK inhibitor SB, a drug that reportedly reverses A $\beta$ -induced synaptic impairments in mice (Saleshando and O'Connor, 2000; Guo et al., 2017), and measured Panx1-dependent EtBr uptake. As shown in **Figure 5B**, SB significantly reduced Panx1 activity in Tg slices, suggesting that p38MAPK also favors Panx1 activation in the AD context. These results suggest that a "positive loop" between Panx1 and p38MAPK exacerbates their activities, amplifying A $\beta$ -induced neurotoxicity in AD (**Figure 6**).

## DISCUSSION

AD is a progressive age-related neurodegenerative condition manifested as a severe deterioration of cognitive functions (Selkoe, 2001). sA $\beta$ os have been pointed as responsible for the synaptopathy that occurs early in the pathology, causing defects in neuronal morphology (Lacor et al., 2007; Price et al.,

2014), alterations in receptor trafficking (Hsieh et al., 2006; Miñano-Molina et al., 2011; Baglietto-Vargas et al., 2018), and consequently impairing excitatory synaptic transmission and plasticity (Sheng et al., 2012). Here, we show that Panx1, a nonselective transmembrane channel that connects intracellular and extracellular spaces (MacVicar and Thompson, 2010), is implicated in the sA $\beta$ os-induced early synaptic dysfunction observed in a mouse model of AD. In this regard, our data demonstrate that Panx1 is overexpressed in the hippocampal tissue of Tg compared to Wt mice (**Figure 1**), accumulating in neurons and reactive astrocytes in close proximity to the amyloid plaques (**Figure 1C** and **Supplementary Figure S1**), strongly suggesting its association with the A $\beta$ -induced toxicity. Remarkably, the age-dependent overexpression of Panx1 significantly correlates with the A $\beta$  levels in Tg hippocampal tissue (**Figure 1B**), supporting the idea that A $\beta$  accumulation causes Panx1 overexpression in the AD context. Our results also show an exacerbated Panx1 activity in the hippocampal tissue of the Tg mice upon basal conditions (**Figure 1D**) and upon the induction of glutamate-transmission with NMDA and DHPG (**Figure 1E**), which is normalized by the treatment with PBN. Other authors have suggested previously the involvement of Panx1 in the A $\beta$ -induced neurotoxic signaling in the AD neuropathology. Orellana et al. (2011b) reported that the exogenous application of the A $\beta$  peptide in acute hippocampal slices produces neuronal death in a way dependent on glial hemichannel activity and neuronal Panx1 overactivation (Orellana et al., 2011a,b). How does A $\beta$  signaling promote an aberrant function of Panx1 channels? As proposed by Orellana et al. (2011a), A $\beta$  induces microglia activation and the release of factors that potentially promote connexin hemichannel and Panx1 channel opening in astrocytes, causing a nonregulated release of gliotransmitters such as ATP and glutamate, which in turn increases neuronal excitability, triggering neurotoxic cascades (Orellana et al., 2011a,b). Moreover, Panx1 overactivity has also been involved in the A $\beta$ -triggered degranulation of mast cells (Harcha et al., 2015) and in the aberrant gliotransmission that promotes early inflammatory processes in AD mouse models (Yi et al., 2016, 2017), suggesting that neuro-inflammation could directly increase Panx1 expression and activation in the brains of Tg mice. In fact, although it has not been demonstrated in brains, pro-inflammatory stimuli such as interleukin (IL)-1 $\beta$  (Negoro et al., 2013) upregulate Panx1 expression, further supporting this idea. Besides neuro-inflammation, the A $\beta$  peptide can directly impact glutamate receptors, enhancing excitatory synaptic transmission. A $\beta$  signaling has been shown to affect synaptic plasticity by inhibiting LTP (Walsh et al., 2002; Wang et al., 2002) at the expense of enhancing NMDAR- (Kim et al., 2001; Hsieh et al., 2006; Li et al., 2009) and mGluR5-dependent LTD (Chen et al., 2013; Hu et al., 2014). Since Panx1 overactivation has been widely associated with aberrant glutamatergic transmission in several neuropathological conditions (Thompson et al., 2008; Lopatár et al., 2015; Dossi et al., 2018), it is feasible that A $\beta$  upregulates Panx1 activity through a mechanism involving NMDAR and mGluR5 activation. In this regard, it has been demonstrated that Panx1 opening is triggered by the activation of NMDA and mGlu5 glutamate receptors, leading to epileptiform

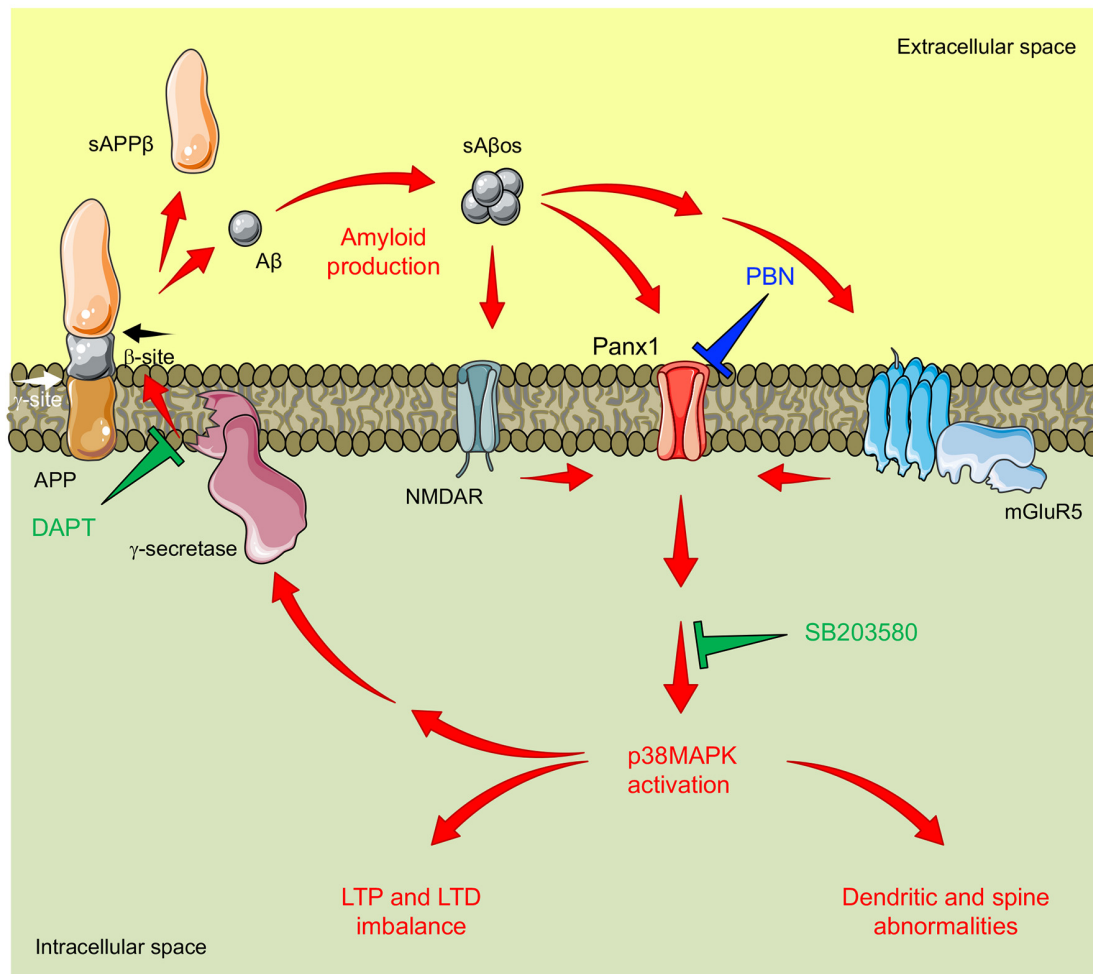


**FIGURE 6 |** Proposed model for pannexin 1 (Panx1)'s role in AD synaptotoxicity. Amyloid  $\beta$  peptide ( $A\beta$ ) is generated by the proteolytic cleavage of the amyloid precursor protein (APP). This processing is executed by the consecutive actions of  $\beta$ -secretase (not shown) and  $\gamma$ -secretase resulting in the release of a soluble  $\beta$ -cleaved APP fragment (sAPP $\beta$ ) and the  $A\beta$ , respectively.  $A\beta$  can form soluble oligomeric aggregates (sA $\beta$ os) that easily diffuse and bind to several postsynaptic partners including N-methyl-D-aspartate receptors (NMDARs) and type 1 metabotropic glutamate receptor 5 (mGluR5), enhancing glutamatergic transmission and promoting NMDAR/mGluR5-mediated activation of Panx1 channels. Panx1 overactivity favors signaling cascades that promote the activation (phosphorylation) of p38-MAPK (p38MAPK), a kinase involved in the early stages of the  $A\beta$ -induced synaptic dysfunction in AD. In turn, p38MAPK promotes  $A\beta$  production and accumulation, further increasing Panx1 overactivity and producing a "positive loop" that amplifies the  $A\beta$ -induced neurotoxicity. Congruently with this mechanism, the inhibition of Panx1 with probenecid (PBN) reverses p38MAPK activation and improves LTP/LTD and structural impairments in the AD model brain. Similarly, inhibition of p38MAPK with SB208035 (SB) or the inhibition of  $\gamma$ -secretase with N-[N-(3,5-difluorophenacetyl-L-alanyl)]-S-phenylglycine t-butyl ester (DAPT) reduces Panx1 overactivity.

activity in hippocampal neurons (Thompson et al., 2008; Lopatár et al., 2015). More recently, it was shown that Panx1 activity directly contributes to the generation of seizures in human epileptic brain tissues (Dossi et al., 2018). Notably, in all these cases, the pharmacological blockade of Panx1 channels produces an anticonvulsant effect, suggesting that inhibiting Panx1 is an efficient strategy to ameliorate an exacerbated excitatory synaptic transmission. In this regard, the observations that the Panx1 blocker PBN (Silverman et al., 2008) is capable of reversing LTP and LTD impairments in Tg hippocampal slices (Figures 3A–D) support the idea that an exacerbated Panx1 activity could be an important player in the early synaptic dysfunction that affects AD brains. In fact, acute treatment with

PBN does not have a significant impact on neurodegeneration parameters such as  $A\beta$  deposition, astrogliosis, or neuronal death (Figure 2), further suggesting that Panx1 overactivity becomes more relevant in the initial synaptotoxic mechanisms in AD.

In order to evaluate downstream effectors of the Panx1 overactivity, we estimated the activation of p38MAPK. This tau kinase is overexpressed and becomes overactive during normal aging, as well as in age-related neurodegenerative diseases such as AD (Hensley et al., 1999). Particularly, p38 $\alpha$ -MAPK is overexpressed at early stages of AD neuropathology (Sun et al., 2003) and appears to mediate early cascades that lead to neuroinflammation, synaptic dysfunction, and spatial memory defects in AD models (Munoz et al., 2007). Consequently, its



inhibition reduces microglial production of pro-inflammatory cytokines and improves synaptic and cognitive functions in A $\beta$ -treated mice (Munoz et al., 2007) and in AD genetic models (Roy et al., 2015). In agreement with the fact that PBN improves LTP/LTD defects in Tg hippocampal slices (**Figure 3**), our results show that the acute inhibition of Panx1 with PBN significantly reduces p38MAPK activation (**Figure 5A**), suggesting that Panx1 overactivity contributes to the neurotoxic signaling that leads to p38MAPK activation in AD. In 2017, Colié et al. (2017) demonstrated that the specific neuronal ablation of p38MAPK improves synaptic plasticity and memory performances in an AD model. These authors showed that such effects rely on the reduction of A $\beta$  accumulation (Colié et al., 2017). Interestingly, we do not observe a significant effect of PBN in the A $\beta$  accumulation and deposition (**Figures 2A–C**), although it has a clear effect on p38MAPK activation (**Figure 5A**). Perhaps the impact of reducing p38MAPK activity on the A $\beta$  aggregation requires a more long-lasting treatment such as the p38MAPK deletion reported by Colié et al. (2017). Nonetheless, its acute inhibition manages to improve LTP defects in A $\beta$ -treated brain slices (Wang et al., 2004; Origlia et al., 2008; Rutigliano et al., 2018), supporting the idea that drugs that reduce p38MAPK activation, such as PBN (**Figure 5A**), could be efficient strategies to improve synaptic defects in the AD context. Interestingly, we also observe that the inhibition of p38MAPK with SB, a drug that reportedly reverses A $\beta$ -induced synaptic impairments in mice (Saleshendo and O'Connor, 2000; Guo et al., 2017), is capable to reduce Panx1 activity in Tg hippocampal slices (**Figure 5B**). Since p38MAPK signaling modulates inflammatory cytokine production (Corrêa and Eales, 2012; Colié et al., 2017) and A $\beta$  accumulation (Colié et al., 2017), two factors that increase Panx1 activation and plasma membrane expression (Orellana et al., 2011b; Negro et al., 2013), it is feasible that a “positive loop” between Panx1 and p38MAPK exacerbates their activities, amplifying A $\beta$ -induced neurotoxicity in AD (**Figure 6**). Indeed, we observe that the treatment with the anti-A $\beta$  drug DAPT, an inhibitor of the  $\gamma$ -secretase complex (Dovey et al., 2001), efficiently reduces Panx1 overactivation in Tg hippocampal slices (**Supplementary Figure S2B**), further supporting the idea that p38MAPK-mediated signaling influences Panx1 activity by promoting A $\beta$  accumulation.

Finally, our results show that the inhibition of Panx1 with PBN not only improves synaptic plasticity (**Figure 3**) but also reverses defects in synaptic structure and dendritic arborization observed in Tg hippocampal tissue (**Figure 4**). These results are in agreement with our idea that targeting Panx1 overactivity is an efficient strategy to ameliorate early functional and structural synaptic defects in the AD context. Surprisingly, PBN is also able to increase dendritic arborization, bringing the number of branches and dendritic length in Tg hippocampal neurons at levels similar to those exhibited by Wt neurons (**Figure 4**). Although dramatic, a rapid effect of PBN in neurite and axonal extension has been already demonstrated by other authors (Horton et al., 2017). Since we hypothesize that Panx1 overactivation contributes to the A $\beta$ -induced neurotoxic signaling by favoring p38MAPK activity, it is likely that this tau-kinase be involved in the effect of PBN on

dendritic arborization. In fact, p38MAPK activation was recently associated with the mechanisms that induce retardation in the axonal and dendritic outgrowth in offspring mice following maternal neuronal injury (Zhou Y. et al., 2019), supporting the idea that p38MAPK overactivation in the AD context could affect neuronal morphology. As PBN efficiently reduces p38MAPK activation (current **Figure 5A**), it could impact dendritic arborization in Tg hippocampal neurons for the same reason.

Consistent with our observations in spine density, it was recently shown that Panx1 negatively regulates cortical dendritic spine development and network connectivity (Sanchez-Arias et al., 2019); however, the underlying mechanism has not yet been resolved. Which of the synaptic mechanisms governing the induction of synaptic plasticity could be impacted by an exacerbated Panx1 activity? One possibility is neuronal actin network. Actin is the most prominent cytoskeletal protein at synapses which is expressed in both axonal terminals and dendrites (Cingolani and Goda, 2008). It is highly enriched in dendritic spines where its organization and remodeling support structural modifications that accompany functional changes sustaining synaptic plasticity (Matus, 2000; Tada and Sheng, 2006; Gordon-Weeks and Fournier, 2014). Congruently, neuronal actin cytoskeleton dynamics are importantly perturbed in the AD context (Minamide et al., 2000; Bamburg and Bloom, 2009), producing structural defects that consequently lead to synaptic dysfunctions (Hsieh et al., 2006; Lacor et al., 2007; Shankar, 2007; Sheng et al., 2012). Moreover, it has been reported that A $\beta$  induces aberrant actin polymerization, affecting actin dynamics through a mechanism involving p38MAPK activity (Song et al., 2002). Interestingly, Panx1 channels interact with actin filaments (Bhalla-Gehi et al., 2010) and actin-binding proteins (Wicki-Stordeur and Swayne, 2013; Boyce et al., 2014) and have been shown to participate in the modulation of actin-dependent changes in neuronal morphology (Wicki-Stordeur and Swayne, 2013; Sanchez-Arias et al., 2019). This latter, added to our observations that PBN reverses a deficient dendritic branching and spine density in the Tg hippocampal tissue (**Figure 4**), strongly suggests that synaptic defects in the AD context rely on Panx1-induced signaling producing actin-dependent structural defects. Further experiments are necessary to confirm this hypothesis.

According to our knowledge, this is the first time that Panx1 is described as a potential target in the early synaptotoxic signaling linked to AD. Furthermore, we provide additional support to the current use of PBN as an emerging tool in clinical and basic research (Colín-González and Santamaría, 2013). PBN is a drug widely used clinically to treat gout and hyperuricemia and also used as a coadjuvant to prolong the actions of antibiotic agents (Robbins et al., 2012; Colín-González and Santamaría, 2013). However, it is necessary to note that PBN targets not only Panx1 channels but also other molecules highly expressed at the central nervous system (CNS). Among them, the organic anion transporter 1 (OAT1; Chiba et al., 2011) and the transient receptor potential vanilloid 2 (TRPV2; Bang et al., 2007). Therefore, side effects in brain tissue cannot be ruled out. Nonetheless,

PBN has been reported to protect from the excitotoxicity induced by sAβos (Carrillo-Mora et al., 2010) and from the inflammatory conditions in CNS (Wei et al., 2015; Hainz et al., 2017; Zhang et al., 2019). Interestingly, PBN can cross the blood–brain barrier, acting directly on the CNS (Kartzinel et al., 1976; Cowdry et al., 1983) and have been shown to exert neuroprotective effects in several neuropathological contexts including cerebral ischemia–reperfusion (Wei et al., 2015), autoimmune encephalomyelitis (Hainz et al., 2016), sepsis-associated encephalopathy (Zhang et al., 2019), multiple sclerosis (Hainz et al., 2017), and epilepsy (Dossi et al., 2018). Moreover, recent studies reported that gout patients treated with different uricosurics including PBN, exhibit lower risk of developing nonvascular dementia (Hong et al., 2015) and AD (Lu et al., 2016). Although the direct effect of PBN on the cognitive status of AD patients has not yet been evaluated, the fact that in our conditions PBN has positive effects on the early synaptic defects observed in hippocampal tissue of Tg mice paves the way to evaluate in the future its impact on cognitive defects in the AD context.

## DATA AVAILABILITY STATEMENT

The datasets used and analyzed during the current study are available from corresponding authors on a reasonable request.

## ETHICS STATEMENT

The use and care of the animals were approved by the Ethics and Animal Care Committee of the Universidad de Valparaíso (BEA064-2015).

## AUTHOR CONTRIBUTIONS

CF-M performed the experiments and critically revised the manuscript. BG, EM, IG, PMuj, and DL-E performed the experiments. PMuñ, CC, CD-A, CH, and AG-J contributed

new reagents/analytic tools and critically revised the manuscript. AG-J wrote the manuscript. AA conceived and designed the experiments and wrote the manuscript. All the authors read and approved the final manuscript.

## FUNDING

This work was supported by Fondo Nacional de Desarrollo Científico y Tecnológico (FONDECYT) N°11150776 (AA), FONDECYT 11180731 (AG-J), FONDECYT 11160760 (CD-A), FONDECYT 11180186 (CH), Millennium Institute P09-022-F (AA and AG-J), Millennium Institute P09-015-F (CH), PAI N°79150045 (AA), REDI170583 (CD-A), Alzheimer's Association Research Grant 2018-AARG-591107 (CD-A), FONDAP (Comisión Nacional de Investigación Científica y Tecnológica) program 15150012 (CH), Fondo de Fomento al Desarrollo Científico y Tecnológico (FONDEF) ID16I10223, and Comisión Nacional de Investigación Científica y Tecnológica (CONICYT)-Brazil 441921/2016-7 (CH) and undergraduate fellowship from PMI-UVA 1402 (BG and EM). Using resources from these funds, reagents were purchased for the experimental development of this research.

## ACKNOWLEDGMENTS

We thank Dr. Nibaldo Inestrosa (Pontificia Universidad Católica de Chile) for kindly providing us with the first cohort of Tg mice used in this study. We also thank Dr. Andrew Quest (Universidad de Chile) for providing us the  $\gamma$ -secretase inhibitor DAPT and Dr. Kathleen Whitlock for providing us the mouse anti-GFAP antibody.

## SUPPLEMENTARY MATERIAL

The Supplementary Material for this article can be found online at: <https://www.frontiersin.org/articles/10.3389/fncel.2020.00046/full#supplementary-material>.

## REFERENCES

- Ardiles, A. O., Flores-Muñoz, C., Toro-Ayala, G., Cárdenas, A. M., Palacios, A. G., Muñoz, P., et al. (2014). Pannexin 1 regulates bidirectional hippocampal synaptic plasticity in adult mice. *Front. Cell. Neurosci.* 8:326. doi: 10.3389/fncel.2014.00326
- Ardiles, A. O., Tapia-Rojas, C. C., Mandal, M., Alexandre, F., Kirkwood, A., Inestrosa, N. C., et al. (2012). Postsynaptic dysfunction is associated with spatial and object recognition memory loss in a natural model of Alzheimer's disease. *Proc. Natl. Acad. Sci. U S A* 109, 13835–13840. doi: 10.1073/pnas.1201209109
- Baglietto-Vargas, D., Prieto, G. A., Limon, A., Forner, S., Rodríguez-Ortiz, C. J., Ikemura, K., et al. (2018). Impaired AMPA signaling and cytoskeletal alterations induce early synaptic dysfunction in a mouse model of Alzheimer's disease. *Aging Cell* 17:e12791. doi: 10.1111/acer.12791
- Bamburg, J. R., and Bloom, G. S. (2009). Cytoskeletal pathologies of Alzheimer disease. *Cell Motil. Cytoskeleton* 66, 635–649. doi: 10.1002/cm.20388
- Bang, S., Kim, K. Y., Yoo, S., Lee, S. H., and Hwang, S. W. (2007). Transient receptor potential V2 expressed in sensory neurons is activated by probenecid. *Neurosci. Lett.* 425, 120–125. doi: 10.1016/j.neulet.2007.08.035
- Bhalla-Gehi, R., Penuela, S., Churko, J. M., Shao, Q., and Laird, D. W. (2010). Pannexin1 and pannexin3 delivery, cell surface dynamics and cytoskeletal interactions. *J. Biol. Chem.* 285, 9147–9160. doi: 10.1074/jbc.m109.082008
- Boyce, A. K., Wicki-Stordeur, L. E., and Swayne, L. A. (2014). Powerful partnership: crosstalk between pannexin 1 and the cytoskeleton. *Front. Physiol.* 5:27. doi: 10.3389/fphys.2014.00027
- Busche, M. A., Chen, X., Henning, H. A., Reichwald, J., Staufenbiel, M., Sakmann, B., et al. (2012). Critical role of soluble amyloid- $\beta$  for early hippocampal hyperactivity in a mouse model of Alzheimer's disease. *Proc. Natl. Acad. Sci. U S A* 109, 8740–8745. doi: 10.1073/pnas.1206171109
- Carrillo-Mora, P., Mendez-Cuesta, L. A., Perez-De La Cruz, V., Fortoul-van Der Goes, T. I., and Santamaria, A. (2010). Protective effect of systemic L-kynurenine and probenecid administration on behavioural and morphological alterations induced by toxic soluble amyloid  $\beta$  (25–35) in rat hippocampus. *Behav. Brain Res.* 210, 240–250. doi: 10.1016/j.bbr.2010.02.041
- Chen, X., Lin, R., Chang, L., Xu, S., Wei, X., Zhang, J., et al. (2013). Enhancement of long-term depression by soluble amyloid  $\beta$  protein in rat hippocampus

- is mediated by metabotropic glutamate receptor and involves activation of p38MAPK, STEP and caspase-3. *Neuroscience* 253, 435–443. doi: 10.1016/j.neuroscience.2013.08.054
- Chiba, S., Ikawa, T., Takeshita, H., Ichiba, K., Sagi, M., Mukai, T., et al. (2011). Interactions of human organic anion transporter 1 (hOAT1) with substances associated with forensic toxicology. *Leg. Med.* 13, 180–185. doi: 10.1016/j.legalmed.2011.04.001
- Cingolani, L. A., and Goda, Y. (2008). Actin in action: the interplay between the actin cytoskeleton and synaptic efficacy. *Nat. Rev. Neurosci.* 9, 344–356. doi: 10.1038/nrn2373
- Cleary, J. P., Walsh, D. M., Hofmeister, J. J., Shankar, G. M., Kuskowski, M. A., Selkoe, D. J., et al. (2005). Natural oligomers of the amyloid- $\beta$  protein specifically disrupt cognitive function. *Nat. Neurosci.* 8, 79–84. doi: 10.1038/nn1372
- Colié, S., Sarroca, S., Palenzuela, R., Garcia, I., Matheu, A., Corpas, R., et al. (2017). Neuronal p38 $\alpha$  mediates synaptic and cognitive dysfunction in an Alzheimer's mouse model by controlling  $\beta$ -amyloid production. *Sci. Rep.* 7:45306. doi: 10.1038/srep45306
- Colín-González, A. L., and Santamaría, A. (2013). Probenecid: an emerging tool for neuroprotection. *CNS Neurol. Disord. Drug Targets* 12, 1050–1065. doi: 10.2174/18715273113129990090
- Collingridge, G. L., Peineau, S., Howland, J. G., and Wang, Y. T. (2010). Long term depression in the CNS. *Nat. Rev. Neurosci.* 11, 459–473. doi: 10.1038/nrn2867
- Corrêa, S. A., and Eales, K. L. (2012). The role of p38 MAPK and its substrates in neuronal plasticity and neurodegenerative disease. *J. Signal Transduct.* 2012:649079. doi: 10.1155/2012/649079
- Cowdry, R. W., Ebert, M. H., van Kammen, D. P., Post, R. M., and Goodwin, F. K. (1983). Cerebrospinal fluid probenecid studies: a reinterpretation. *Biol. Psychiatry* 18, 1287–1299.
- DeKosky, S. T., and Scheff, S. W. (1990). Synapse loss in frontal cortex biopsies in Alzheimer's disease: correlation with cognitive severity. *Ann. Neurol.* 27, 457–464. doi: 10.1002/ana.410270502
- Dossi, E., Blauwblomme, T., Moulard, J., Chever, O., Vasile, F., Guinard, E., et al. (2018). Pannexin-1 channels contribute to seizure generation in human epileptic brain tissue and in a mouse model of epilepsy. *Sci. Transl. Med.* 10:eaar3796. doi: 10.1126/scitranslmed.aar3796
- Dovey, H. F., John, V., Anderson, J. P., Chen, L. Z., de Saint Andrieu, P., Fang, L. Y., et al. (2001). Functional  $\gamma$ -secretase inhibitors reduce  $\beta$ -amyloid peptide levels in brain. *J. Neurochem.* 76, 173–181. doi: 10.1046/j.1471-4159.2001.00012.x
- Duyckaerts, C., Potier, M. C., and Delatour, B. (2008). Alzheimer disease models and human neuropathology: similarities and differences. *Acta Neuropathol.* 115, 5–38. doi: 10.1007/s00401-007-0312-8
- Fornier, S., Baglietto-Vargas, D., Martini, A. C., Trujillo-Estrada, L., and LaFerla, F. M. (2017). Synaptic impairment in Alzheimer's disease: a dysregulated symphony. *Trends Neurosci.* 40, 347–357. doi: 10.1016/j.tins.2017.04.002
- Fukumoto, H., Tokuda, T., Kasai, T., Ishigami, N., Hidaka, H., Kondo, M., et al. (2010). High-molecular-weight  $\beta$ -amyloid oligomers are elevated in cerebrospinal fluid of Alzheimer patients. *FASEB J.* 24, 2716–2726. doi: 10.1096/fj.09-150359
- Gajardo, I., Salazar, C. S., Lopez-Espindola, D., Estay, C., Flores-Munoz, C., Elgueta, C., et al. (2018). Lack of pannexin 1 alters synaptic GluN2 subunit composition and spatial reversal learning in mice. *Front. Mol. Neurosci.* 11:114. doi: 10.3389/fnmol.2018.00114
- Gogolla, N., Galimberti, I., and Caroni, P. (2007). Structural plasticity of axon terminals in the adult. *Curr. Opin. Neurobiol.* 17, 516–524. doi: 10.1016/j.conb.2007.09.002
- Gomez-Arboledas, A., Davila, J. C., Sanchez-Mejias, E., Navarro, V., Nunez-Diaz, C., Sanchez-Varo, R., et al. (2018). Phagocytic clearance of presynaptic dystrophies by reactive astrocytes in Alzheimer's disease. *Glia* 66, 637–653. doi: 10.1002/glia.23270
- Gong, Y., Chang, L., Viola, K. L., Lacor, P. N., Lambert, M. P., Finch, C. E., et al. (2003). Alzheimer's disease-affected brain: presence of oligomeric A $\beta$  ligands (ADDLs) suggests a molecular basis for reversible memory loss. *Proc. Natl. Acad. Sci. U S A* 100, 10417–10422. doi: 10.1073/pnas.1834302100
- Gordon-Weeks, P. R., and Fournier, A. E. (2014). Neuronal cytoskeleton in synaptic plasticity and regeneration. *J. Neurochem.* 129, 206–212. doi: 10.1111/jnc.12502
- Götz, J., and Ittner, L. M. (2008). Animal models of Alzheimer's disease and frontotemporal dementia. *Nat. Rev. Neurosci.* 9, 532–544. doi: 10.1038/nrn2420
- Guo, J., Chang, L., Li, C., Li, M., Yan, P., Guo, Z., et al. (2017). SB203580 reverses memory deficits and depression-like behavior induced by microinjection of A $\beta$ 1–42 into hippocampus of mice. *Metab. Brain Dis.* 32, 57–68. doi: 10.1007/s11011-016-9880-4
- Hainz, N., Wolf, S., Beck, A., Wagenpfeil, S., Tschernig, T., and Meier, C. (2017). Probenecid arrests the progression of pronounced clinical symptoms in a mouse model of multiple sclerosis. *Sci. Rep.* 7:17214. doi: 10.1038/s41598-017-17517-5
- Hainz, N., Wolf, S., Tschernig, T., and Meier, C. (2016). Probenecid application prevents clinical symptoms and inflammation in experimental autoimmune encephalomyelitis. *Inflammation* 39, 123–128. doi: 10.1007/s10753-015-0230-1
- Harcha, P. A., Vargas, A., Yi, C., Koulakoff, A. A., Giaume, C., and Saez, J. C. (2015). Hemichannels are required for amyloid  $\beta$ -peptide-induced degranulation and are activated in brain mast cells of APP<sup>swe</sup>/PS1<sup>DE9</sup> mice. *J. Neurosci.* 35, 9526–9538. doi: 10.1523/jneurosci.3686-14.2015
- Harris, K. M., Fiala, J. C., and Ostroff, L. (2003). Structural changes at dendritic spine synapses during long-term potentiation. *Philos. Trans. R. Soc. Lond. B Biol. Sci.* 358, 745–748. doi: 10.1098/rstb.2002.1254
- Hensley, K., Floyd, R. A., Zheng, N. Y., Nael, R., Robinson, K. A., Nguyen, X., et al. (1999). p38 kinase is activated in the Alzheimer's disease brain. *J. Neurochem.* 72, 2053–2058. doi: 10.1046/j.1471-4159.1999.0722053.x
- Hong, J. Y., Lan, T. Y., Tang, G. J., Tang, C. H., Chen, T. J., and Lin, H. Y. (2015). Gout and the risk of dementia: a nationwide population-based cohort study. *Arthritis Res. Ther.* 17:139. doi: 10.1186/s13075-015-0642-1
- Horton, S. M., Luna Lopez, C., Blevins, E., Howarth, H., Weisberg, J., Shestopalov, V. I., et al. (2017). Pannexin 1 modulates axonal growth in mouse peripheral nerves. *Front. Cell. Neurosci.* 11:365. doi: 10.3389/fncel.2017.00365
- Hsieh, H., Boehm, J., Sato, C., Iwatsubo, T., Tomita, T., Sisodia, S., et al. (2006). AMPAR removal underlies A $\beta$ -induced synaptic depression and dendritic spine loss. *Neuron* 52, 831–843. doi: 10.1016/j.neuron.2006.10.035
- Hu, N. W., Nicoll, A. J., Zhang, D., Mably, A. J., O'Malley, T., Purro, S. A., et al. (2014). mGlu5 receptors and cellular prion protein mediate amyloid- $\beta$ -facilitated synaptic long-term depression *in vivo*. *Nat. Commun.* 5:3374. doi: 10.1038/ncomms4374
- Huang, Y., Grinspan, J. B., Abrams, C. K., and Scherer, S. S. (2007). Pannexin1 is expressed by neurons and glia but does not form functional gap junctions. *Glia* 55, 46–56. doi: 10.1002/glia.20435
- Jankowsky, J. L., Fadale, D. J., Anderson, J., Xu, G. M., Gonzales, V., Jenkins, N. A., et al. (2004). Mutant presenilins specifically elevate the levels of the 42 residue  $\beta$ -amyloid peptide *in vivo*: evidence for augmentation of a 42-specific  $\gamma$  secretase. *Hum. Mol. Genet.* 13, 159–170. doi: 10.1093/hmg/ddh019
- Kartzinel, R., Ebert, M. H., and Chase, T. N. (1976). Intravenous probenecid loading. Effects on plasma and cerebrospinal fluid probenecid levels and on monoamine metabolites in cerebrospinal fluid. *Neurology* 26, 992–996. doi: 10.1212/wnl.26.10.992
- Kessels, H. W., Nabavi, S., and Malinow, R. (2013). Metabotropic NMDA receptor function is required for  $\beta$ -amyloid-induced synaptic depression. *Proc. Natl. Acad. Sci. U S A* 110, 4033–4038. doi: 10.1073/pnas.1219605110
- Kim, J. H., Anwyl, R., Suh, Y. H., Djamgoz, M. B., and Rowan, M. J. (2001). Use-dependent effects of amyloidogenic fragments of  $\beta$ -amyloid precursor protein on synaptic plasticity in rat hippocampus *in vivo*. *J. Neurosci.* 21, 1327–1333. doi: 10.1523/jneurosci.21-04-01327.2001
- Klyubin, I., Betts, V., Welzel, A. T., Blennow, K., Zetterberg, H., Wallin, A., et al. (2008). Amyloid  $\beta$  protein dimer-containing human CSF disrupts synaptic plasticity: prevention by systemic passive immunization. *J. Neurosci.* 28, 4231–4237. doi: 10.1523/JNEUROSCI.5161-07.2008
- Lacor, P. N., Buniel, M. C., Furlow, P. W., Clemente, A. S., Velasco, P. T., Wood, M., et al. (2007). A $\beta$  oligomer-induced aberrations in synapse composition, shape and density provide a molecular basis for loss of connectivity in Alzheimer's disease. *J. Neurosci.* 27, 796–807. doi: 10.1523/jneurosci.3501-06.2007
- Li, S., Hong, S., Shepardson, N. E., Walsh, D. M., Shankar, G. M., and Selkoe, D. (2009). Soluble oligomers of amyloid  $\beta$  protein facilitate hippocampal



- long-term depression by disrupting neuronal glutamate uptake. *Neuron* 62, 788–801. doi: 10.1016/j.neuron.2009.05.012
- Li, S., Jin, M., Koeglsperger, T., Shepardson, N. E., Shankar, G. M., and Selkoe, D. J. (2011). Soluble A $\beta$  oligomers inhibit long-term potentiation through a mechanism involving excessive activation of extrasynaptic NR2B-containing NMDA receptors. *J. Neurosci.* 31, 6627–6638. doi: 10.1523/JNEUROSCI.0203-11.2011
- Lopátár, J., Dale, N., and Frenguelli, B. G. (2015). Pannexin-1-mediated ATP release from area CA3 drives mGlu5-dependent neuronal oscillations. *Neuropharmacology* 93, 219–228. doi: 10.1016/j.neuropharm.2015.01.014
- Lu, N., Dubreuil, M., Zhang, Y., Neogi, T., Rai, S. K., Ascherio, A., et al. (2016). Gout and the risk of Alzheimer's disease: a population-based, BMI-matched cohort study. *Ann. Rheum. Dis.* 75, 547–551. doi: 10.1136/annrheumdis-2014-206917
- Lynch, M. A. (2004). Long-term potentiation and memory. *Physiol. Rev.* 84, 87–136. doi: 10.1152/physrev.00014.2003
- MacVicar, B. A., and Thompson, R. J. (2010). Non-junction functions of pannexin-1 channels. *Trends Neurosci.* 33, 93–102. doi: 10.1016/j.tins.2009.11.007
- Malenka, R. C., and Bear, M. F. (2004). LTP and LTD: an embarrassment of riches. *Neuron* 44, 5–21. doi: 10.1016/j.neuron.2004.09.012
- Matus, A. (2000). Actin-based plasticity in dendritic spines. *Science* 290, 754–758. doi: 10.1126/science.290.5492.754
- McGeer, E. G., and McGeer, P. L. (2003). Inflammatory processes in Alzheimer's disease. *Prog. Neuropsychopharmacol. Biol. Psychiatry* 27, 741–749. doi: 10.1016/S0278-5846(03)00124-6
- Minamide, L. S., Striegl, A. M., Boyle, J. A., Meberg, P. J., and Bamburg, J. R. (2000). Neurodegenerative stimuli induce persistent ADF/cofilin-actin rods that disrupt distal neurite function. *Nat. Cell Biol.* 2, 628–636. doi: 10.1038/35023579
- Miñano-Molina, A. J., España, J., Martín, E., Barneda-Zahonero, B., Fadó, R., Solé, M., et al. (2011). Soluble oligomers of amyloid- $\beta$  peptide disrupt membrane trafficking of  $\alpha$ -amino-3-hydroxy-5-methylisoxazole-4-propionic acid receptor contributing to early synapse dysfunction. *J. Biol. Chem.* 286, 27311–27321. doi: 10.1074/jbc.M111.227504
- Morra, J. H., Tu, Z., Apostolova, L. G., Green, A. E., Avedissian, C., Madsen, S. K., et al. (2009). Automated 3D mapping of hippocampal atrophy and its clinical correlates in 400 subjects with Alzheimer's disease, mild cognitive impairment and elderly controls. *Hum. Brain Mapp.* 30, 2766–2788. doi: 10.1002/hbm.20708
- Mucke, L., Masliah, E., Yu, G. Q., Mallory, M., Rockenstein, E. M., Tatsuno, G., et al. (2000). High-level neuronal expression of a $\beta$  1–42 in wild-type human amyloid protein precursor transgenic mice: synaptotoxicity without plaque formation. *J. Neurosci.* 20, 4050–4058. doi: 10.1523/jneurosci.20-11-04050.2000
- Munoz, L., Ralay Ranaivo, H., Roy, S. M., Hu, W., Craft, J. M., McNamara, L. K., et al. (2007). A novel p38  $\alpha$  MAPK inhibitor suppresses brain proinflammatory cytokine up-regulation and attenuates synaptic dysfunction and behavioral deficits in an Alzheimer's disease mouse model. *J. Neuroinflammation* 4:21. doi: 10.1186/1742-2094-4-21
- Negoro, H., Lutz, S. E., Liou, L. S., Kanematsu, A., Ogawa, O., Scemes, E., et al. (2013). Pannexin 1 involvement in bladder dysfunction in a multiple sclerosis model. *Sci. Rep.* 3:2152. doi: 10.1038/srep02152
- Nelson, P. T., Alafuzoff, I., Bigio, E. H., Bouras, C., Braak, H., Cairns, N. J., et al. (2012). Correlation of Alzheimer disease neuropathologic changes with cognitive status: a review of the literature. *J. Neuropathol. Exp. Neurol.* 71, 362–381. doi: 10.1097/NEN.0b013e31825018f7
- Orellana, J. A., Froger, N., Ezan, P., Jiang, J. X., Bennett, M. V., Naus, C. C., et al. (2011a). ATP and glutamate released via astroglial connexin 43 hemichannels mediate neuronal death through activation of pannexin 1 hemichannels. *J. Neurochem.* 118, 826–840. doi: 10.1111/j.1471-4159.2011.07210.x
- Orellana, J. A., Shoji, K. F., Abudara, V., Ezan, P., Amigou, E., Saez, P. J., et al. (2011b). Amyloid  $\beta$ -induced death in neurons involves glial and neuronal hemichannels. *J. Neurosci.* 31, 4962–4977. doi: 10.1523/JNEUROSCI.6417-10.2011
- Origlia, N., Righi, M., Capsoni, S., Cattaneo, A., Fang, F., Stern, D. M., et al. (2008). Receptor for advanced glycation end product-dependent activation of p38 mitogen-activated protein kinase contributes to amyloid- $\beta$ -mediated cortical synaptic dysfunction. *J. Neurosci.* 28, 3521–3530. doi: 10.1523/JNEUROSCI.0204-08.2008
- Palop, J. J., Chin, J., Roberson, E. D., Wang, J., Thwin, M. T., Bien-Ly, N., et al. (2007). Aberrant excitatory neuronal activity and compensatory remodeling of inhibitory hippocampal circuits in mouse models of Alzheimer's disease. *Neuron* 55, 697–711. doi: 10.1016/j.neuron.2007.07.025
- Peng, G. P., Feng, Z., He, F. P., Chen, Z. Q., Liu, X. Y., Liu, P., et al. (2015). Correlation of hippocampal volume and cognitive performances in patients with either mild cognitive impairment or Alzheimer's disease. *CNS Neurosci. Ther.* 21, 15–22. doi: 10.1111/cns.12317
- Philipson, O., Lord, A., Gumucio, A., O'Callaghan, P., Lannfelt, L., and Nilsson, L. N. (2010). Animal models of amyloid- $\beta$ -related pathologies in Alzheimer's disease. *FEBS J.* 277, 1389–1409. doi: 10.1111/j.1742-4658.2010.07564.x
- Price, K. A., Varghese, M., Sowa, A., Yuk, F., Brautigam, H., Ehrlich, M. E., et al. (2014). Altered synaptic structure in the hippocampus in a mouse model of Alzheimer's disease with soluble amyloid- $\beta$  oligomers and no plaque pathology. *Mol. Neurodegener.* 9:41. doi: 10.1186/1750-1326-9-41
- Rammes, G., Hasenjäger, A., Sroka-Saidi, K., Deussing, J. M., and Parsons, C. G. (2011). Therapeutic significance of NR2B-containing NMDA receptors and mGluR5 metabotropic glutamate receptors in mediating the synaptotoxic effects of  $\beta$ -amyloid oligomers on long-term potentiation (LTP) in murine hippocampal slices. *Neuropharmacology* 60, 982–990. doi: 10.1016/j.neuropharm.2011.01.051
- Reed, M. N., Hofmeister, J. J., Jungbauer, L., Welzel, A. T., Yu, C., Sherman, M. A., et al. (2011). Cognitive effects of cell-derived and synthetically derived A $\beta$  oligomers. *Neurobiol. Aging* 32, 1784–1794. doi: 10.1016/j.neurobiolaging.2009.11.007
- Robbins, N., Koch, S. E., Tranter, M., and Rubinstein, J. (2012). The history and future of probenecid. *Cardiovasc. Toxicol.* 12, 1–9. doi: 10.1007/s12012-011-9145-8
- Roy, S. M., Grum-Tokars, V. L., Schavocky, J. P., Saeed, F., Staniszewski, A., Teich, A. F., et al. (2015). Targeting human central nervous system protein kinases: an isoform selective p38 $\alpha$ MAPK inhibitor that attenuates disease progression in Alzheimer's disease mouse models. *ACS Chem. Neurosci.* 6, 666–680. doi: 10.1021/acschemneuro.5b00002
- Rutigliano, G., Stazi, M., Arancio, O., Watterson, D. M., and Origlia, N. (2018). An isoform-selective p38 $\alpha$  mitogen-activated protein kinase inhibitor rescues early entorhinal cortex dysfunctions in a mouse model of Alzheimer's disease. *Neurobiol. Aging* 70, 86–91. doi: 10.1016/j.neurobiolaging.2018.06.006
- Saleshando, G., and O'Connor, J. J. (2000). SB203580, the p38 mitogen-activated protein kinase inhibitor blocks the inhibitory effect of  $\beta$ -amyloid on long-term potentiation in the rat hippocampus. *Neurosci. Lett.* 288, 119–122. doi: 10.1016/s0304-3940(00)01210-6
- Sanchez-Arias, J. C., Liu, M., Choi, C. S. W., Ebert, S. N., Brown, C. E., and Swayne, L. A. (2019). Pannexin 1 regulates network ensembles and dendritic spine development in cortical neurons. *eNeuro* 6:ENEURO.0503-18.2019. doi: 10.1523/ENEURO.0503-18.2019
- Segal, M. (2005). Dendritic spines and long-term plasticity. *Nat. Rev. Neurosci.* 6, 277–284. doi: 10.1038/nrn1649
- Selkoe, D. J. (2001). Alzheimer's disease: genes, proteins and therapy. *Physiol. Rev.* 81, 741–766. doi: 10.1152/physrev.2001.81.2.741
- Selkoe, D. J. (2008). Soluble oligomers of the amyloid  $\beta$ -protein impair synaptic plasticity and behavior. *Behav. Brain Res.* 192, 106–113. doi: 10.1016/j.bbr.2008.02.016
- Shankar, G. M. E. A. (2007). Natural oligomers of the Alzheimer amyloid- $\beta$  protein induce reversible synapse loss by modulating an NMDA-type glutamate receptor-dependent signaling pathway. *J. Neurosci.* 27, 2866–2875. doi: 10.1523/JNEUROSCI.4970-06.2007
- Shankar, G. M., Li, S., Mehta, T. H., Garcia-Munoz, A., Shepardson, N. E., Smith, I., et al. (2008). Amyloid- $\beta$  protein dimers isolated directly from Alzheimer's brains impair synaptic plasticity and memory. *Nat. Med.* 14, 837–842. doi: 10.1038/nm1782
- Sheng, M., Sabatini, B. L., and Sudhof, T. C. (2012). Synapses and Alzheimer's disease. *Cold Spring Harb. Perspect. Biol.* 4:a005777. doi: 10.1101/cshperspect.a005777

- Silverman, W. R., de Rivero Vaccari, J. P., Locovei, S., Qiu, F., Carlsson, S. K., Scemes, E., et al. (2009). The pannexin 1 channel activates the inflammasome in neurons and astrocytes. *J. Biol. Chem.* 284, 18143–18151. doi: 10.1074/jbc.M109.004804
- Silverman, W., Locovei, S., and Dahl, G. (2008). Probenecid, a gout remedy, inhibits pannexin 1 channels. *Am. J. Physiol. Cell Physiol.* 295, C761–C767. doi: 10.1152/ajpcell.00227.2008
- Snyder, E. M., Nong, Y., Almeida, C. G., Paul, S., Moran, T., Choi, E. Y., et al. (2005). Regulation of NMDA receptor trafficking by amyloid- $\beta$ . *Nat. Neurosci.* 8, 1051–1058. doi: 10.1038/nn1503
- Song, C., Perides, G., Wang, D., and Liu, Y. F. (2002).  $\beta$ -Amyloid peptide induces formation of actin stress fibers through p38 mitogen-activated protein kinase. *J. Neurochem.* 83, 828–836. doi: 10.1046/j.1471-4159.2002.01182.x
- Sun, A., Liu, M., Nguyen, X. V., and Bing, G. (2003). P38 MAP kinase is activated at early stages in Alzheimer's disease brain. *Exp. Neurol.* 183, 394–405. doi: 10.1016/s0014-4886(03)00180-8
- Tada, T., and Sheng, M. (2006). Molecular mechanisms of dendritic spine morphogenesis. *Curr. Opin. Neurobiol.* 16, 95–101. doi: 10.1016/j.conb.2005.12.001
- Takeuchi, T., Duszakiewicz, A. J., and Morris, R. G. (2014). The synaptic plasticity and memory hypothesis: encoding, storage and persistence. *Philos. Trans. R. Soc. Lond. B Biol. Sci.* 369:20130288. doi: 10.1098/rstb.2013.0288
- Tamburri, A., Dudilot, A., Licea, S., Bourgeois, C., and Boehm, J. (2013). NMDA-receptor activation but not ion flux is required for amyloid- $\beta$  induced synaptic depression. *PLoS One* 8:e65350. doi: 10.1371/journal.pone.0065350
- Terry, R. D., Masliah, E., Salmon, D. P., Butters, N., DeTeresa, R., Hill, R., et al. (1991). Physical basis of cognitive alterations in Alzheimer's disease: synapse loss is the major correlate of cognitive impairment. *Ann. Neurol.* 30, 572–580. doi: 10.1002/ana.410300410
- Thompson, R. J., Jackson, M. F., Olah, M. E., Rungta, R. L., Hines, D. J., Beazely, M. A., et al. (2008). Activation of pannexin-1 hemichannels augments aberrant bursting in the hippocampus. *Science* 322, 1555–1559. doi: 10.1126/science.1165209
- Townsend, M., Shankar, G. M., Mehta, T., Walsh, D. M., and Selkoe, D. J. (2006). Effects of secreted oligomers of amyloid  $\beta$ -protein on hippocampal synaptic plasticity: a potent role for trimers. *J. Physiol.* 572, 477–492. doi: 10.1113/jphysiol.2005.103754
- Vogt, A., Hormuzdi, S. G., and Monyer, H. (2005). Pannexin1 and Pannexin2 expression in the developing and mature rat brain. *Mol. Brain Res.* 141, 113–120. doi: 10.1016/j.molbrainres.2005.08.002
- Walsh, D. M., Klyubin, I., Fadeeva, J. V., Cullen, W. K., Anwyl, R., Wolfe, M. S., et al. (2002). Naturally secreted oligomers of amyloid  $\beta$  protein potently inhibit hippocampal long-term potentiation *in vivo*. *Nature* 416, 535–539. doi: 10.1038/416535a
- Wang, H. W., Pasternak, J. F., Kuo, H., Ristic, H., Lambert, M. P., Chromy, B., et al. (2002). Soluble oligomers of  $\beta$  amyloid (1–42) inhibit long-term potentiation but not long-term depression in rat dentate gyrus. *Brain Res.* 924, 133–140. doi: 10.1016/s0006-8993(01)03058-x
- Wang, Q., Walsh, D. M., Rowan, M. J., Selkoe, D. J., and Anwyl, R. (2004). Block of long-term potentiation by naturally secreted and synthetic amyloid  $\beta$ -peptide in hippocampal slices is mediated *via* activation of the kinases c-Jun N-terminal kinase, cyclin-dependent kinase 5 and p38 mitogen-activated protein kinase as well as metabotropic glutamate receptor type 5. *J. Neurosci.* 24, 3370–3378. doi: 10.1523/JNEUROSCI.1633-03.2004
- Wei, R., Wang, J., Xu, Y., Yin, B., He, F., Du, Y., et al. (2015). Probenecid protects against cerebral ischemia/reperfusion injury by inhibiting lysosomal and inflammatory damage in rats. *Neuroscience* 301, 168–177. doi: 10.1016/j.neuroscience.2015.05.070
- Wicki-Stordeur, L. E., and Swayne, L. A. (2013). Panx1 regulates neural stem and progenitor cell behaviours associated with cytoskeletal dynamics and interacts with multiple cytoskeletal elements. *Cell Commun. Signal.* 11:62. doi: 10.1186/1478-811X-11-62
- Yi, C., Ezan, P., Fernandez, P., Schmitt, J., Saez, J. C., Giaume, C., et al. (2017). Inhibition of glial hemichannels by boldine treatment reduces neuronal suffering in a murine model of Alzheimer's disease. *Glia* 65, 1607–1625. doi: 10.1002/glia.23182
- Yi, C., Mei, X., Ezan, P., Mato, S., Matias, I., Giaume, C., et al. (2016). Astroglial connexin43 contributes to neuronal suffering in a mouse model of Alzheimer's disease. *Cell Death Differ.* 23, 1691–1701. doi: 10.1038/cdd.2016.63
- Zhang, Z., Lei, Y., Yan, C., Mei, X., Jiang, T., Ma, Z., et al. (2019). Probenecid relieves cerebral dysfunction of sepsis by inhibiting pannexin 1-dependent ATP release. *Inflammation* 42, 1082–1092. doi: 10.1007/s10753-019-00969-4
- Zhou, K. Q., Green, C. R., Bennet, L., Gunn, A. J., and Davidson, J. O. (2019). The role of connexin and pannexin channels in perinatal brain injury and inflammation. *Front. Physiol.* 10:141. doi: 10.3389/fphys.2019.00141
- Zhou, Y., Ji, J., Chen, C., and Hong, F. (2019). Retardation of axonal and dendritic outgrowth is associated with the mapk signaling pathway in offspring mice following maternal exposure to nanosized titanium dioxide. *J. Agric. Food Chem.* 67, 2709–2715. doi: 10.1021/acs.jafc.8b06992

**Conflict of Interest:** The authors declare that the research was conducted in the absence of any commercial or financial relationships that could be construed as a potential conflict of interest.

Copyright © 2020 Flores-Muñoz, Gómez, Mery, Mujica, Gajardo, Córdova, Lopez-Espindola, Durán-Aniotz, Hetz, Muñoz, Gonzalez-Jamett and Ardiles. This is an open-access article distributed under the terms of the Creative Commons Attribution License (CC BY). The use, distribution or reproduction in other forums is permitted, provided the original author(s) and the copyright owner(s) are credited and that the original publication in this journal is cited, in accordance with accepted academic practice. No use, distribution or reproduction is permitted which does not comply with these terms.